atmosphere

MDPI

Article

Changes in Regional Extreme Cold Events over Northern China and Their Circulation Associations Under Arctic Amplification

Yu Zhang [1,2] and Jinqi Li [1,2,*]

[1] College of Aviation Meteorology, Civil Aviation Flight University of China, Guanghan 618307, China; zhangyu198303@163.com
[2] China Meteorological Administration Key Laboratory for Aviation Meteorology, Guanghan 618307, China
* Correspondence: ljq13948052763@163.com

Abstract

In recent decades, rapid Arctic warming has intensified Arctic amplification (AA), and its potential impacts on mid-latitude extreme weather events have received increasing attention. Using meteorological station observations and reanalysis datasets from 1979 to 2024, this study investigates the variations of regional extreme cold events (RECEs) over Northern China and their associated circulation characteristics under different Arctic amplification periods. The Arctic amplification index (AAI850), Siberian High Index (SHI), Ural Ridge Index (URI), and multi-scale atmospheric circulation fields are employed to examine the relationships between Arctic thermal conditions and Eurasian atmospheric circulation anomalies. The results show that: (1) During the study period, AAI850 showed a significant upward trend, while the frequency of RECEs in northern China decreased significantly. At the same time, the cold intensity of the event minimum temperature and the composite intensity of RECEs were significantly enhanced, reflecting a shift from a high-frequency/weak-anomaly mode to a low-frequency/high-intensity mode. (2) In the later Arctic amplification period, the distribution of RECEs shifted toward lower minimum temperatures, the event center moved northward, and the duration structure changed modestly, while the affected area showed no significant change. These findings indicate that the intensification of RECEs is mainly associated with enhanced cold-anomaly intensity, rather than prolonged duration or expanded spatial coverage. (3) AAI850 shows significant correlations with Siberian High and Ural ridge anomalies, suggesting a close association between Arctic amplification and high-latitude circulation anomalies in Eurasia. (4) The circulation analysis reveals widespread increases in 500 hPa geopotential height over the Arctic and Eurasia, regional differences in sea-level pressure changes, and warmer conditions at 850 hPa during the later Arctic amplification period. Nevertheless, northwesterly or northerly wind components persist over parts of northern China, suggesting that southward cold-air transport remains possible despite the warmer thermal background.

Keywords: Arctic amplification; regional extreme cold events; Siberian High; Ural blocking; northern China

Academic Editor: Gareth Marshall

Received: 4 October 2026
Revised: 1 November 2026
Accepted: 3 November 2026
Published: 5 November 2026

Copyright: © 2026 by the authors. Licensee MDPI, Basel, Switzerland. This article is an open access article distributed under the terms and conditions of the Creative Commons Attribution (CC BY) license.

1. Introduction

In recent decades, the global climate system has undergone significant changes, among which the warming rate in the Arctic region far exceeds the global average, thus

triggering a typical phenomenon called "Arctic Amplification" (AA) [1–3]. Arctic amplification is one of the most prominent features of modern climate change, mainly manifested in the rapid rise of near-surface temperature in the Arctic, accompanied by a series of climate system responses, including the reduction in sea ice, the reduction in surface albedo, and the enhancement of atmospheric and ocean feedback processes [2,4–6]. Although the indicators that measure the amplification of the Arctic vary in definition and calculation methods, they all reflect the abnormal warming characteristics of the Arctic relative to mid- and low latitudes [7]. As an important part of the global climate system, the rapid warming of the Arctic not only changes the regional thermal condition and sea ice environment but also may affect the weather and climate of mid-latitudes by adjusting the temperature gradients in the poles and mid-latitudes, affecting the rapid structure, and changing the large-scale atmospheric circulation background [1,6,8]. Therefore, Arctic amplification and its impact on mid-latitude climate anomalies have become an important topic in the field of climate change research.

Previous studies have shown that the signal of the amplification effect of the Arctic has continued to strengthen in recent decades, and the warming characteristics since the beginning of the 21st century have been more prominent [3,8]. Chylek et al. (2022) pointed out that the Arctic amplification index was roughly maintained between 2 and 3 between 1970 and 2000, but the index rose to more than 4 in the first two decades of the 21st century, indicating that the Arctic amplification was further enhanced after the beginning of the 21st century [9]. Recent studies have further indicated that the Arctic troposphere has undergone sustained warming since the 1990s, with Arctic amplification (AA) reaching relatively high levels in the early 2000s. This period coincided with the maximum rates of sea ice area, thickness, and volume loss [10]. Based on satellite passive microwave observations beginning in October 1978, Arctic sea ice extent has exhibited a declining linear trend in all months [11]. Data from the Copernicus Climate Change Service indicate that the rate of decline in Arctic sea ice extent has varied considerably over time, with the most rapid decline occurring in the late 1990s and early 2000s. Since 2007, the declining trend has become less pronounced, but September sea ice extent has consistently remained below the 1991–2020 reference-period average [12]. The reduction in sea ice is considered to be an important factor in aggravating the warming of the Arctic, because it further amplifies the regional warming effect by reducing the surface albedo, changing the sea-gas heat exchange process and adjusting the atmospheric feedback mechanism [1,5,13]. Based on the above-mentioned changes in the climate background, this study chooses around 2000 as the boundary point of inter-annual comparison, and defines 1979–2000 and 2001–2024 as periods of relatively weak and enhanced Arctic amplification, aiming to explore how regional extreme cold events change under different Arctic amplification backgrounds. The changing characteristics of these events under different AA backgrounds. It should be noted that this division is mainly aimed at building a comparative framework for climate response in different Arctic amplification contexts, which does not mean that 2000 is a turning point for the sudden change in the intensity of Arctic amplification.

Arctic amplification not only changes the average state of the climate but also may affect the characteristics of extreme weather events in mid-latitudes. Among them, extreme cold events, as a climate anomaly with a wide impact and significant social consequences, continue to occur in the context of global warming and have received wide attention [8,14]. Although the global average temperature has risen, regional extreme cold events have not completely disappeared; their changes are jointly regulated by climate background conditions and large-scale atmospheric circulation anomalies [15–17]. Past studies have shown that Arctic amplification may affect mid-latitude circulation abnormalities in multiple ways [14,18,19]. Some studies point out that warming in high

latitudes may affect the conditions of abnormal cold events by changing the background of winter circulation in Eurasia [20]. However, there is still controversy in the academic community about the relationship between Arctic amplification and extreme cold events in mid-latitudes. Some studies believe that Arctic amplification may enhance specific circulation abnormalities and affect the occurrence of extreme cold events [14,18]; other studies argue that the change in mid-latitude cold events is mainly controlled by a variety of climatic factors, and there are significant regional differences in the influence of Arctic amplification [16,17,21]. Therefore, against the background of the continuous warming in the Arctic, whether extreme cold events show systematic changes, and how the corresponding large-scale circulation background is adjusted, still needs to be studied in depth.

Northern China is located in the mid- and high latitudes of East Asia, which is an important area affected by winter cold air activity. The extreme cold events in the region are jointly affected by the cold air activity of Eurasia and the anomalies of atmospheric circulation at mid- and high latitudes [22,23]. Because this region is located on an important path of Eurasian cold air southward and is more sensitive to changes in mid- and high-latitude circulation, it is an ideal area for studying the response characteristics of regional extreme cold events under the background of Arctic amplification. Previous studies have shown that winter climate anomalies in East Asia are closely related to the Siberian High, changes in winter winds in East Asia, and the adjustment of high-latitude circulation in Eurasia [22]. As an important system affecting the winter wind in East Asia, the Siberian High can regulate the intensity of the cold air source and the transportation of cold air to East Asia, thus affecting the cold events in East Asia [22]. In addition, the Barents–Kara sea ice anomaly can regulate cold events by affecting the background of winter circulation in Eurasia [20]; while the abnormal blockage of the Ural Mountains can change the circulation structure of the mid- and high latitudes of Eurasia, affecting the transmission path and holding of cold air. Over time, it is associated with extreme cold events in Eurasia [24,25]. Therefore, the formation and development of extreme cold events in northern China are not controlled by a single circulation system, but by the joint regulation of high-latitude cold air activity, mid–high-latitude circulation anomalies in Eurasia and the East Asian winter wind system.

Reanalysis datasets provide an important basis for examining winter atmospheric circulation and its relationship with extreme cold events. Recent studies have used ERA5 to investigate the circulation processes associated with cold extremes over East Asia and Eurasia. Zhuo et al. combined ERA5 reanalysis with model experiments to examine the responses of atmospheric blocking and East Asian cold extremes to Arctic sea-ice loss, highlighting the role of circulation anomalies over eastern Siberia [26]. Ye et al. used ERA5 temperature, geopotential height, sea-level pressure, and wind fields to characterize the record-breaking cold event over eastern China in December 2023 and quantify the contribution of large-scale atmospheric circulation to its intensity [27]. Zhang et al. combined ERA5 and other datasets with numerical experiments to investigate consecutive extreme cold spells over Eurasia, revealing connections among snow-cover anomalies, atmospheric circulation, and cold-air accumulation over Siberia [28]. These studies demonstrate the value of reanalysis data for linking surface cold extremes with their large-scale circulation backgrounds. Accordingly, the present study combines long-term station observations with ERA5 reanalysis: station observations are used to identify and characterize regional extreme cold events over northern China, while ERA5 provides the atmospheric fields needed to examine the associated mid- and high-latitude circulation patterns. This complementary use of observations and reanalysis supports an integrated assessment of event characteristics, statistical relationships with Arctic amplification, and circulation backgrounds.

Although previous studies have widely explored the relationship between Arctic amplification and mid-latitude cold events, there is still a lack of systematic understanding of the multiple characteristic changes of regional extreme cold events under the background of Arctic amplification and their circulation links [29]. First of all, previous studies have focused on the cold wave process or single-station extreme cold changes, while regional extreme cold events involve the synchronous occurrence and continuous development of cold anomalies within a certain space, and their characteristics cannot be fully described by a single site or a single temperature indicator. Research on extreme climate events shows that comprehensive consideration of multiple characteristics such as frequency, intensity and duration helps to a more comprehensive understanding of changes in extreme climate events [30,31]. Gong et al. (2012) proposed a regional low-temperature extreme event identification method that comprehensively considers temperature anomalies, spatial continuity and duration, which can effectively depict regional-scale extreme cold events [32]. Therefore, it is necessary to study the changing characteristics of regional extreme cold events against the background of Arctic amplification based on the regional identification method from multiple dimensions such as frequency, cold anomaly intensity, duration and spatial range.

Secondly, although previous studies have explored the relationship between Arctic amplification and extreme cold events in mid-latitudes, it is not clear whether the frequency and intensity changes of regional extreme cold events show consistent characteristics against the background of the strengthening of Arctic amplification. In the context of global warming, extreme cold events have not completely disappeared, and their changes may be affected by changes in the Arctic environment and large-scale circulation abnormalities [14,17]. Therefore, it is necessary to use long-term observation datasets to further compare the differences in multiple characteristics of regional extreme cold events in different Arctic amplification periods. In addition, regional extreme cold events are closely related to key circulation systems in the mid- and high latitudes of Eurasia. However, under the background of Arctic amplification, the link between key circulation anomalies and changes in extreme cold events, as well as the differences in large-scale circulation backgrounds in different Arctic amplification periods, still needs to be studied in depth. Therefore, it is necessary to comprehensively use the Arctic amplification index, key circulation indicators and multi-scale atmospheric circulation fields to deeply understand the changing characteristics of regional extreme cold events from the two dimensions of statistical relationship and circulation background.

To address these questions, this study uses station observations and reanalysis datasets for the cold seasons from 1979/80 to 2023/24 (November to March of the following year), and applies the regional extreme cold event identification method of Gong et al. (2012) [32] to northern China. On this basis, the Arctic amplification index (AAI850), Siberian High Index (SHI), Ural Ridge Index (URI), and multi-scale atmospheric circulation fields are used to examine regional extreme cold events and their circulation relationships under different Arctic amplification periods. Specifically, this study aims to: (1) analyze changes in the frequency, cold-anomaly intensity, duration, and spatial extent of regional extreme cold events under different Arctic amplification periods; (2) explore statistical relationships among Arctic amplification indices, key circulation anomalies, and regional extreme cold event indices; and (3) compare 500 hPa geopotential height, sea level pressure, and 850 hPa temperature/geopotential-height/wind fields during extreme cold events under different Arctic amplification periods, thereby revealing large-scale circulation background changes.

2. Materials and Methods

Based on meteorological station observation data and ERA5 reanalysis data, this study explores the spatial and temporal evolution characteristics of regional extreme cold events (RECEs) in northern China under the background of Arctic amplification (AA) and their related large-scale circulation anomalies.

2.1. Data and Material Description

This study uses the daily minimum temperature observation data from China's meteorological stations. The research period covers the cold seasons from November 1979 to March 2024, with each cold season defined as November of a given year to March of the following year. In order to identify regional extreme cold events, this study selected 974 weather stations in northern China.

The division of northern China is based on the description of the characteristics of China's climate zoning by Zhu and Lu [33]. This study defines the northern region of China as: 35° N–55° N and 73° E–135° E. The region mainly includes Northeast China, North China, Inner Mongolia and the eastern part of the northwest. The region is deeply affected by winter Siberian High activity, East Asian winter wind changes, and winter southward cold air outbreaks.

The reanalysis data are from ERA5 (https://cds.climate.copernicus.eu/datasets (accessed on 16 November 2025)) [34]. ERA5 covers the cold seasons from 1979/80 to 2023/24, with each cold season defined as November of the previous year to March of the following year, and a horizontal resolution of 1° × 1°. This study begins in November 1979, consistent with previous studies on Arctic amplification that adopted 1979 as the starting year. Rantanen et al. noted that more accurate remote sensing observations have provided an important basis for studying Arctic climate change since 1979, a period characterized by pronounced Arctic warming [3]. The study period extends through March 2024, primarily based on the temporal coverage of the meteorological station observations and to ensure the inclusion of the complete 2023/2024 cold season. The ERA5 variables used in this study include: (1) 500 hPa potential height, which is used to analyze the changes in large-scale circulation anomalies in mid- and high latitudes, Eurasian wave column structure and high pressure ridge of the Ural Mountains; (2) 850 hPa temperature, latitude wind, longitude wind and geopotential height, which is used to study the troposphere Low-level temperature abnormalities, cold air activity characteristics, and dynamic and thermal conditions related to the transmission of cold air to northern China; and (3) sea level pressure (MSLP), which is used to analyze changes in the near-surface pressure system, especially the activity and abnormality of Siberian High.

2.2. Identification of Regional Extreme Cold Events and Construction of Atmospheric Circulation Indices

This study adopts the regional extreme cold event identification method proposed by Gong et al. (2012) [32]. Quality control and station screening were performed on the daily minimum temperature observations from more than 1200 meteorological stations in northern China. Stations with anomalous data or incomplete records covering the study period were excluded to ensure data quality and temporal consistency. After screening, 974 stations with complete records for the cold seasons from 1979/80 to 2023/24 were retained for the analysis of regional extreme cold events. Based on the daily minimum temperature observation data of 974 meteorological stations in northern China for the cold seasons of 1979/80–2023/24, regional extreme cold events in northern China under the background of Arctic amplification were identified. The method comprehensively considers the spatial distribution of single-station extreme low-temperature abnormalities,

low-temperature abnormalities and the continuity of regional low-temperature processes, and can objectively identify regional extreme cold events with a certain spatial coverage and duration. Previous studies on extreme cold events have primarily relied on daily observations from individual meteorological stations. Although these methods can identify station-level daily extreme events of meteorological significance, the identification of persistent regional extreme cold events occurring at subseasonal or seasonal timescales often requires manual judgment, resulting in limited efficiency and operational applicability [32]. The regional extreme cold event identification method proposed by Gong et al. (2012) can objectively identify regional events characterized by a certain degree of spatial coherence and temporal persistence according to predefined parameters and consistent criteria, thereby reducing the subjectivity associated with manual identification [32]. In addition, this method provides a relatively comprehensive set of event indices that quantitatively characterize event characteristics in terms of extreme intensity, cumulative cold intensity, affected area, duration, and composite intensity. Therefore, this study adopts this method to identify regional extreme cold events in northern China, providing a basis for subsequent analyses of changes in event frequency, intensity, and spatial extent. The objective identification technique for regional extreme low-temperature events has been applied in studies covering China and Eurasia. Feng et al. used the objective identification technique for regional low-temperature events (OITRLTE) to identify and analyze regional extreme low-temperature events across China during 1960–2013 [35]. Zhang et al. (2021) further applied an improved objective identification technique to investigate long-lasting regional extreme low-temperature events across Eurasia during the winters of 1948/1949–2017/2018 [36]. These studies demonstrate the application of this type of objective identification technique across different spatial scales. Based on the identified events, the characteristic index of regional extreme cold events is constructed. The detailed identification process, index definition, and calculation method are all referred to in the research of Gong et al. (2012) [32]. The definitions of the indices are as follows.

The daily indicators include daily extreme intensity (Q_d, °C), defined here as the minimum of the daily minimum temperatures recorded at all stations within the daily event zone; daily cumulative intensity (L_d, °C); daily affected area (A_d, 10^4 km^2); a composite index (Z_d) integrating these three characteristics; and the daily location of the event center:

$$Q_d = max(T_j), j = 1,2,\cdots,m_d; \quad (1)$$

$$L_d = \sum_j (T_j - T_j^0), j = 1,2,\cdots,m_d; \quad (2)$$

$$A_d = \sum_j a_j, j = 1,2,\cdots,m_d; \quad (3)$$

$$Z_d = e_1 Q_d + e_2 L_d + e_3 A_d, \quad (4)$$

Here, j denotes a station where the daily temperature reaches the extreme-event threshold; T_j^0 is the extreme-event threshold at station j; and j is the number of stations affected on a given day during a regional extreme event. To calculate the daily affected area in Equation (3), the station observations are first mapped onto a 1 °C × 1 °C grid. The variable a_j denotes the area represented by each grid point, and m_d is the number of grid points within the maximum daily affected area during the event. In Equation (4), e_1, e_2, and e_3 are weighting coefficients. This study adopted an equal-weight additive approach to combine four standardized indicators representing minimum temperature, cumulative intensity, affected area, and event duration. Equal weighting is a commonly

used method for constructing composite indicators, particularly when sufficient empirical evidence is unavailable to justify assigning different weights to individual components [37].

These indicators describe the overall characteristics of an extreme low-temperature event, including event extreme intensity (Q, °C), event cumulative intensity (L, °C), cumulative affected area (A, 10^4 km^2), duration (N, days), a composite index (Z), and the location of the center of the event's maximum affected area.

$$Q = max(Q_d), d = 1,2,\cdots,N; \tag{5}$$

$$L = \sum_{i=1}^{n} L_d; \tag{6}$$

$$A_{max} = max(A_d), d = 1,2,\cdots,N; \tag{7}$$

$$A = \sum_{i=1}^{N} A_d, \tag{8}$$

$$Z = e_1 Q + e_2 L + e_3 N + e_4 A. \tag{9}$$

Here, e_1, e_2, e_3 and e_4 in Equation (8) are weighting coefficients. The composite index for the entire event is calculated by first standardizing the daily event indicators and then taking their weighted sum. This study adopted an equal-weight additive approach to combine four standardized indices.

In order to quantitatively characterize the key atmospheric circulation anomalies that affect the regional extreme cold events in northern China under the background of Arctic amplification, this study constructs the Arctic amplification index (AAI850), the Siberian High index (SHI) and the Ural Ridge Index (URI). These indices describe the large-scale circulation background associated with regional extreme cold events from three aspects: abnormal temperature differences between the Arctic and mid-latitudes, near-surface high-pressure system abnormalities, and abnormal middle and upper troposphere circulation.

The typical feature of Arctic amplification is that the warming rate in the Arctic is higher than that in the mid-latitudes. Therefore, previous studies have used Arctic 850 hPa temperature to characterize Arctic amplification and quantified Arctic amplification using the difference in temperature anomalies between the Arctic and lower-latitude regions [38,39]. Francis and Vavrus defined the Arctic region as 70–90° N and the midlatitude region as 30–60° N, and used the difference in near-surface temperature anomalies between the two regions to characterize the temperature contrast between the Arctic and midlatitudes [40]. Following these approaches, this study defines the Arctic amplification index at 850 hPa (AAI850) as the difference between the regional mean 850 hPa temperature anomalies over the Arctic (70–90° N) and the midlatitudes (30–60° N):

$$\mathrm{AAI}_{850} = \overline{\mathrm{T}'_{\mathrm{Arctic}}} - \overline{\mathrm{T}'_{\mathrm{Mid-latitude}}}, \tag{10}$$

where the first term $\overline{\mathrm{T}'_{\mathrm{Arctic}}}$ denotes the regional mean 850 hPa temperature anomaly in the Arctic (70° N–90° N), and the second term $\overline{\mathrm{T}'_{\mathrm{Mid-latitude}}}$ denotes that in the mid-latitudes (30° N–60° N). The increase in AAI850 shows that the temperature increase in the Arctic is more significant than that in mid-latitudes.

The Siberian High is an important near-surface high-pressure system over the Eurasian continent during winter, and its intensity variations play an important role in the East Asian winter monsoon and cold-air outbreak activity. Previous studies have defined the Siberian High Index using regional mean sea level pressure anomalies over

the Siberian region [41,42]. Therefore, the SHI was defined as the regional mean sea level pressure anomaly over 40–60° N and 80–120° E, following the regional domain commonly used in previous studies [41,43]:

$$SHI = \overline{SLP'_{40-60^{\circ}N,80-120^{\circ}E}}, \quad (11)$$

where the term SLP′ denotes the sea level pressure anomaly. The Siberian High region was defined as 40° N–60° N and 80° E–120° E. A positive SHI indicates an enhanced Siberian High.

The Ural region is located in a key area of the mid- and high-latitude circulation system in Eurasia. The 500 hPa geopotential height abnormality in the region can reflect changes in the Ural high-pressure ridge and blocked circulation. Previous studies have shown that the abnormal 500 hPa geopotential height in the Ural-Siberian region is closely related to the abnormal winter circulation in Eurasia [44,45]. Therefore, the URI was defined as the regional mean 500 hPa geopotential height anomaly over 50–70°N and 40–80°E. This domain is consistent with that used in previous studies to characterize 500 hPa geopotential height variations over the Ural region [46]:

$$URI = \overline{Z'_{500,50-70^{\circ}N,40-80^{\circ}E}}, \quad (12)$$

where the term Z'_{500} denotes 500 hPa geopotential height. The Ural region was defined as 50° N–70° N and 40° E–80° E. URI is positive, indicating the enhancement of the Ural high-pressure ridge.

Because AAI850, SHI, and URI are derived from different physical variables and have different units, all indices were standardized before correlation analysis. The standardization method commonly used in climate statistical analysis was applied [47]:

$$X^{*} = \frac{X - \bar{X}}{\sigma}, \quad (13)$$

where the primed symbol denotes the standardized index, and the bar and sigma denote the mean and standard deviation, respectively.

2.3. Arctic Amplification Period Division and Statistical Significance Tests

Based on previous studies of the interdecadal variability of Arctic amplification (AA), this study adopts the winter season of 2000/01 as the boundary between the two comparison periods. Accordingly, the winters of 1979/80–1999/2000 and 2000/01–2023/24 are defined as the early and late periods, respectively. This classification provides a framework for examining changes in regional extreme cold events under different AA backgrounds. It should be noted that the boundary is used for comparative analysis and does not represent a uniquely defined physical turning point in AA or imply that its evolution is attributable to a single driver. The sensitivity of the main results to alternative boundary years was examined by shifting the original boundary 5 and 10 years earlier and later. The results are presented in Supplementary Table S1.

In order to identify change points in the time series, this study adopts the Pettitt non-parametric change point test method. This method was proposed by Pettitt [48] and can detect unknown change points in the time series based on rank statistics.

The statistic is defined as:

$$U_t = 2\sum_{i=1}^{t} R_i - t(n+1), \quad (14)$$

The maximum statistic is:

$$K = \max|U_t|, \quad (15)$$

when $p < 0.05$, the time series was considered to exhibit a statistically significant abrupt change.

In order to evaluate the statistical significance of the differences in the characteristics of regional extreme cold events between different AA (Arctic amplification) stages, this study adopts the Bootstrap resampling method proposed by Efron and Tibshirani [49]. The method constructs the empirical distribution of statistics through random resampling with replacement, and does not need to make assumptions about the potential probability distribution of the sample. Specifically, for the two samples to be compared, independent random resampling is carried out with replacement in their respective samples; the sample volume after resampling is kept consistent with the original sample size, and the corresponding statistics (such as the average or median) of each resampling dataset are calculated. The process is repeated 5000 times to obtain the empirical distribution of the difference between the two statistics, and then calculate the 95% confidence interval based on this distribution. If the confidence interval does not contain zero values, the difference between the two samples is considered to be statistically significant at the 95% confidence level. All the significance tests in this study adopt the above-mentioned Bootstrap method and take the annual events as the resampling unit. For the analysis based on the lag sequence, the significance test results are only used as auxiliary information, and the analysis and interpretation mainly focus on continuous time changes and cumulative change trends.

3. Results

3.1. Changes in Regional Extreme Cold Events over Northern China Under Arctic Amplification

During the study period (cold seasons from 1979/80 to 2023/24), a total of 799 regional extreme cold events in northern China were identified using the objective method of Gong et al. (2012) [32]. The mean latitude and mean longitude of the station records associated with each event were calculated separately, and the resulting coordinates were used to represent the spatial center of that event. Based on this method, the spatial centers of extreme cold events exhibit a distinctly non-uniform spatial distribution across northern China (Figure 1). The center of the incident is mainly concentrated in Xinjiang, central North China and Northeast China, while the frequency of occurrence in the middle area is relatively low. The spatial distribution before and after the occurrence of AA (Arctic amplification) is highly overlapping, indicating that the main areas of the event in the two stages are basically the same. However, there are obvious regional differences in the relative frequency of events, which implies a local redistribution of event activities rather than an overall spatial displacement in a specific direction.

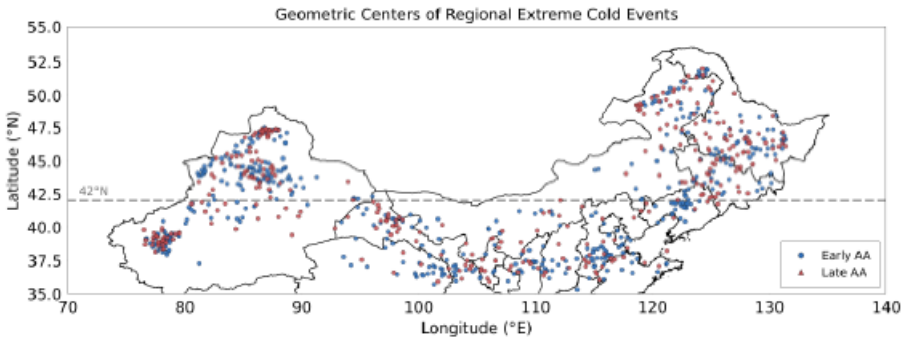


Figure 1. Spatial Distribution of Regional Extreme Low-Temperature Event Centers. Each dot represents the geometric center of an individual regional extreme cold event. Blue dots denote events during the pre-AA period (1979/80–1999/2000), whereas red dots denote events during the post-AA period (2000/01–2023/24). The events were identified based on daily minimum temperature

records from 974 meteorological stations in northern China during the cold seasons from 1979/80 to 2023/24.

Figure 2a shows that the frequency of regional extreme cold events over northern China exhibited pronounced interannual variability over the cold seasons of 1979/80–2023/24. During the pre-AA period, event frequency was generally higher, with several high-frequency years occurring particularly in the 1980s. During the post-AA period, substantial interannual variability persisted, but high-frequency years became less frequent and a clearer downward tendency emerged within the period.

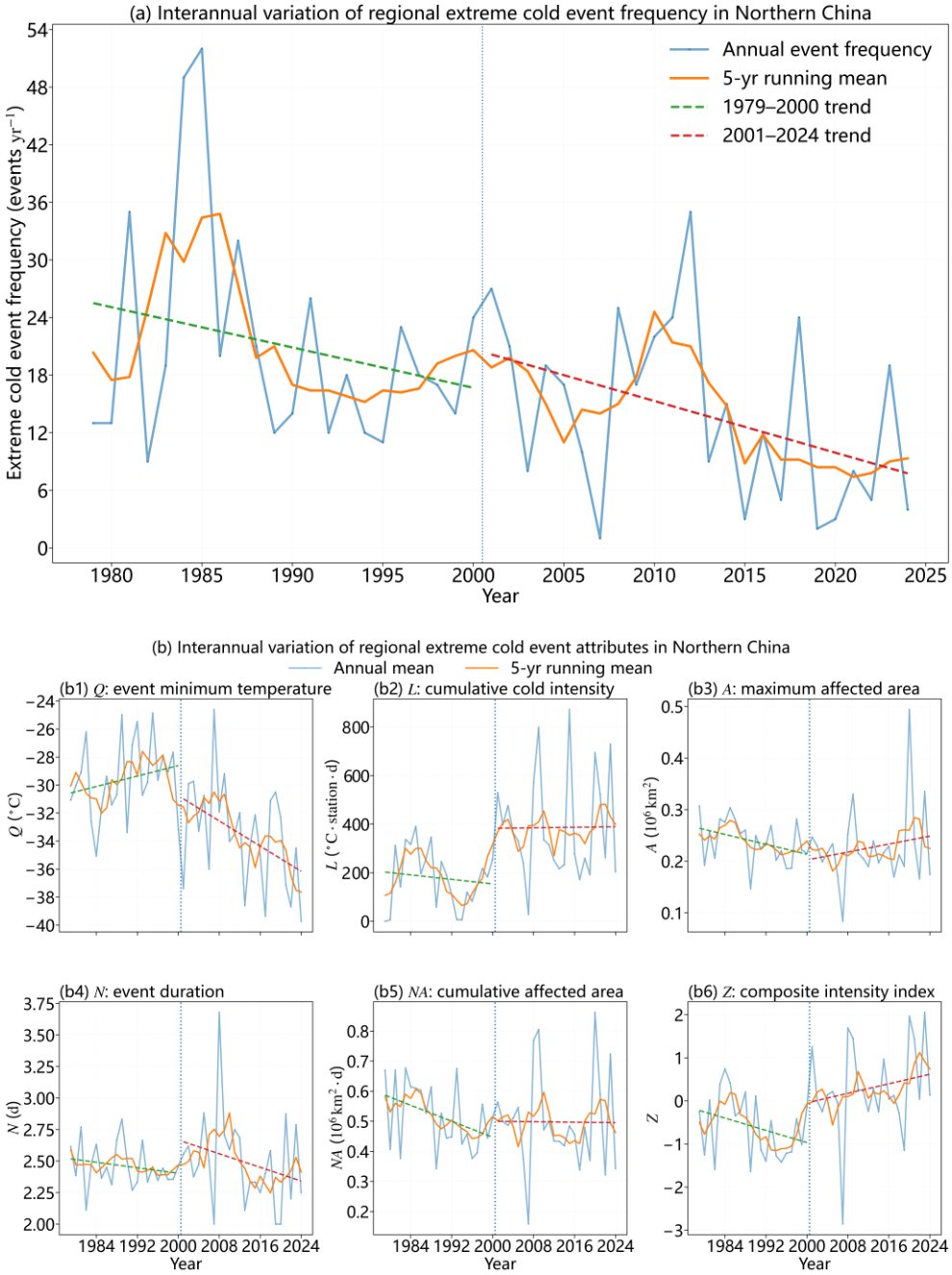
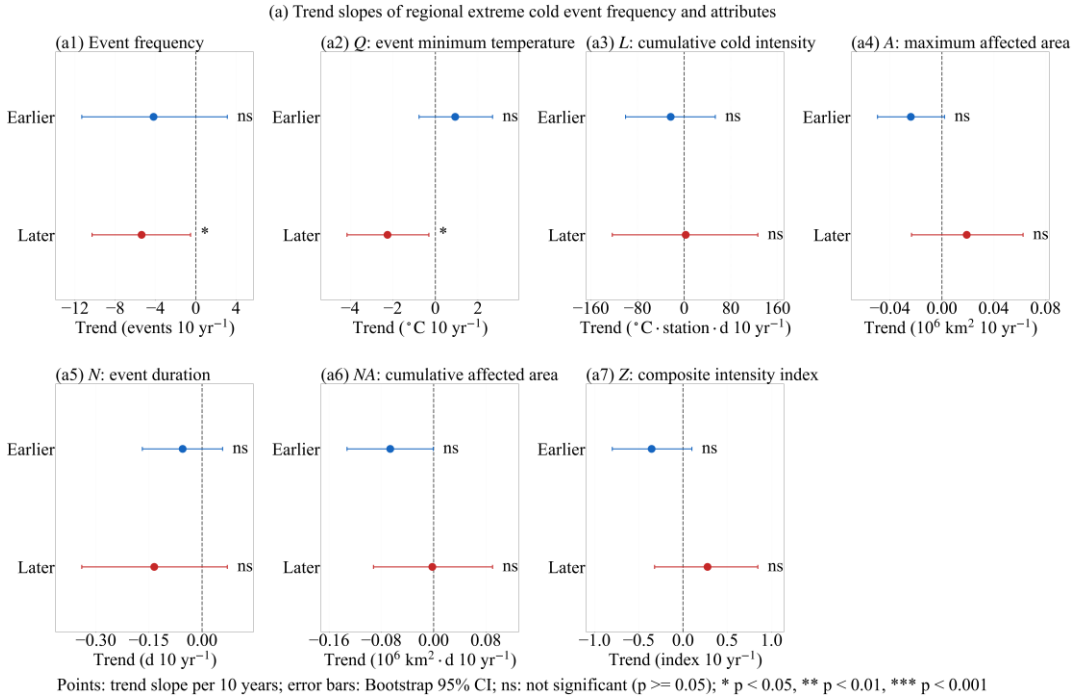


Figure 2. Interannual changes and trends of the frequency and characteristic index of extreme cold events in northern China. (**a**) Interannual changes in the frequency of regional extreme cold events from November 1979 to March 2024. (**b**) Interannual changes in the event characteristic index, including the event minimum temperature *(Q)*, cumulative low temperature intensity *(L)*, maximum impact area *(A)*, event duration *(N)*, cumulative impact area *(NA)* and composite

intensity index *(Z)*. In (**a**,**b**), the orange and green dotted lines represent the linear trend of the period before and after AA, respectively, and the blue vertical dotted lines mark the dividing lines of these two periods. The blue solid line represents the original data.

Different event indicators show completely different evolutionary characteristics in the period before and after AA (Arctic amplification) (Figure 2b). The minimum temperature *(Q)* of the event showed an upward trend before the occurrence of AA, but turned into a downward trend after the occurrence of AA. As shown in Figure 3a, event frequency decreased during the pre-AA period, although the trend was not statistically significant, whereas the decline during the post-AA period was significant ($p < 0.05$). This indicates that the reduction in regional extreme cold event frequency became more evident during the post-AA period. The Pettitt test further identified a significant change point in 2012 ($p = 0.016$), after which the mean event frequency was markedly lower than before the change point (Figure 3(b1)). These results collectively indicate an overall decline in event frequency, accompanied by a pronounced stepwise reduction during the later part of the study period.



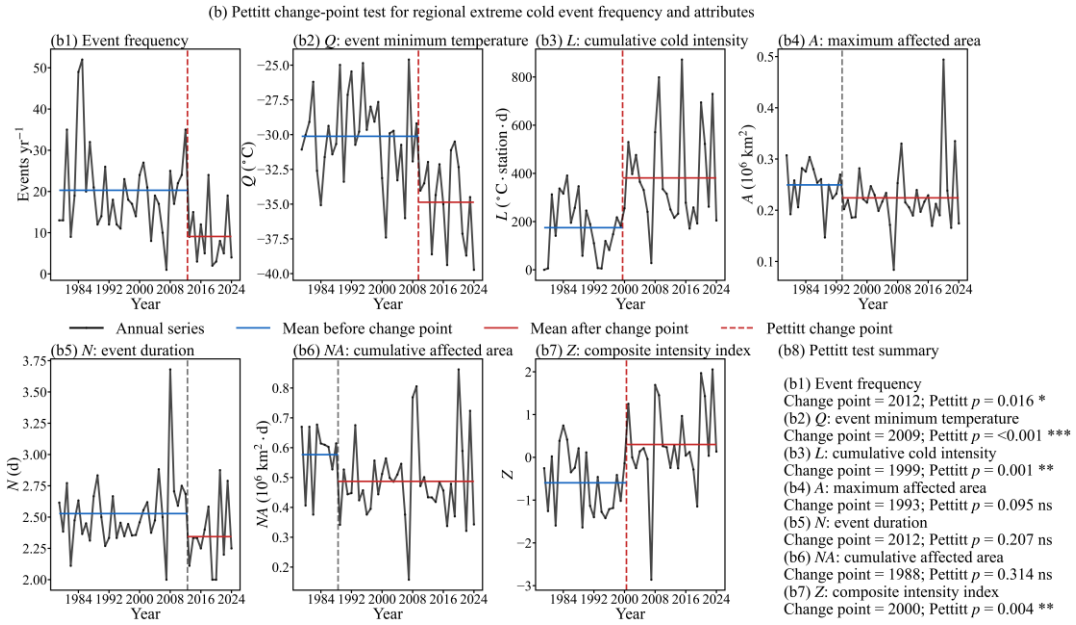


Figure 3. Trends and change-point characteristics of the frequency and characteristic index of extreme cold events in northern China. (**a**) The linear trend slope of the event frequency and characteristic index in the period before and after AA (Arctic amplification), including the event minimum temperature *(Q)*, cumulative low temperature intensity *(L)*, maximum impact area *(A)*, event duration *(N)*, cumulative impact area *(NA)* and composite intensity index *(Z)*. The dot indicates the trend slope per decade, and the error bar represents the 95% confidence interval calculated based on the bootstrap method. The ns indicates that the trend is not significant ($p \geq 0.05$), while *, ** and *** indicate significance at the levels of $p < 0.05$, $p < 0.01$ and $p < 0.001$, respectively. (**b**) The change point of the event frequency and characteristic index identified by the Pettitt test. The black solid line represents the time series year by year, the blue and red horizontal lines represent the average before and after the change point, respectively, and the vertical dotted line indicates the year of the candidate change point; the red line indicates the statistically significant change point ($p < 0.05$), and the gray line indicates the non-remarkable candidate change point. The ns indicates that the trend is not significant ($p \geq 0.05$), while *, ** and *** indicate significance at the levels of $p < 0.05$, $p < 0.01$ and $p < 0.001$, respectively.

It can be seen from Figure 3a that the trend of the minimum temperature *(Q)* before the occurrence of AA is not statistically significant, while the downward trend after the occurrence of AA is significant ($p < 0.05$), indicating that the minimum temperature associated with the regional extreme cold event decreased significantly after the occurrence of AA. The Pettitt test further identified a significant change point in 2009 ($p < 0.001$), and the average minimum temperature after the mutation was significantly lower than before the mutation (Figure 3(b2)), which further confirmed the trend of the change in the lowest temperature of the event to a lower value after AA.

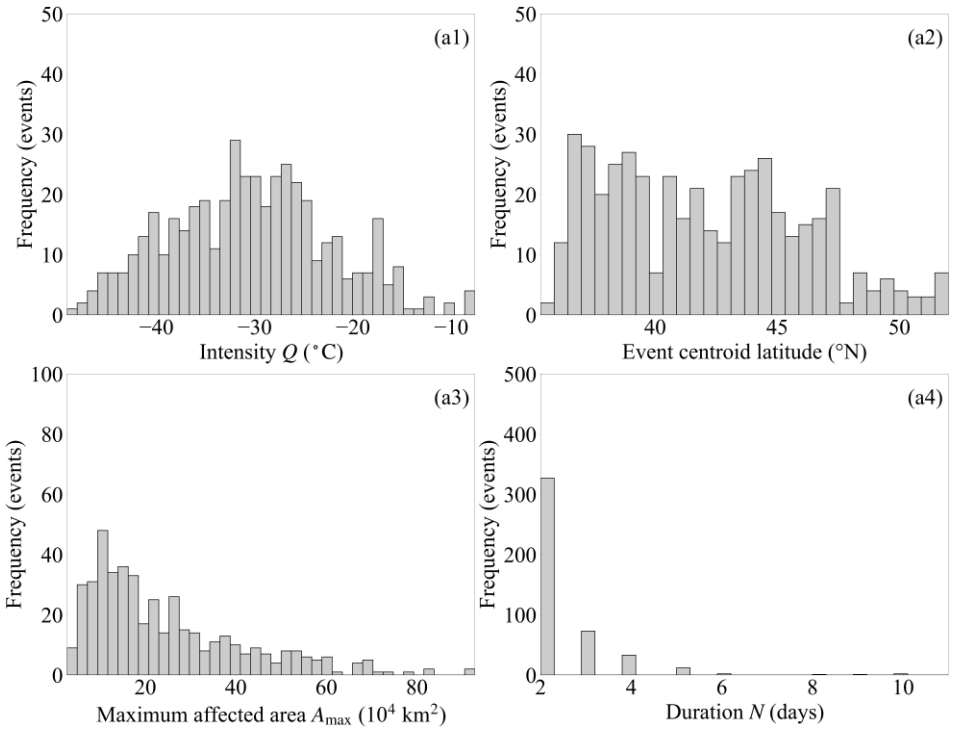
The linear trend of cumulative low temperature intensity *(L)* in each period is not statistically significant; however, the Pettitt test identified a significant change point ($p = 0.001$) in 1999, and the average cumulative low temperature intensity increased significantly after the mutation (Figure 3(b3)). Similarly, the composite intensity index *(Z)* did not show significant linear trends in various periods, but a significant change point ($p = 0.004$) was detected in 2000, and the average after mutation was higher (Figure 3(b7)). These results show that the changing characteristics of *L* and Z are more expressed as step changes in the average state than continuous linear trends. In contrast, although the maximum affected area *(A)*, event duration *(N)* and cumulative affected area *(NA)* identified potential change points in 1993, 2012 and 1988, respectively, according to the

Pettitt test, these change points are not statistically significant (*p*-values of 0.095, 0.207 and 0.314, respectively; Figure 3(b4–b6)). Therefore, these indices should not be interpreted as obvious mutations; in contrast, it is more appropriate to describe their time-change characteristics with interannual fluctuations and insignificant trends.

Overall, Figures 2a and 3b show that there is obvious decoupling between event frequency and intensity-related characteristics during the period after AA (Arctic amplification). The frequency of events decreased significantly and showed a significant step-by-step decrease around 2012; at the same time, the lowest temperature *(Q)* of events also decreased significantly, and a significant mutation occurred in 2009. Although the cumulative low-temperature intensity *(L)* and the composite intensity index *(Z)* did not show a significant linear trend during this period, the average state of the two showed a significant upward leap around 1999 and 2000, respectively. In contrast, no significant change points were detected in the maximum affected area, event duration and cumulative affected area. Overall, these results show that in the period after the occurrence of AA, the frequency of regional extreme cold events decreased, but its minimum temperature tended to be lower, accompanied by the enhancement of other intensity-related indicators or the improvement of the state level.

Figure 4 shows the frequency distribution characteristics of the main attribute indicators of extreme cold events in the early and later regions of the Arctic amplification (AA) effect. These indicators include the lowest temperature of the event *(Q)*, the latitude of the center of mass of the event, the maximum impact area (A_max) and the duration *(N)*. In general, the attribute indicators showed a relatively stable distribution pattern in these two periods, but their responses to different stages of the AA effect differed significantly, indicating that not all characteristics of the evolution of regional extreme cold events changed synchronously.

(a) Distribution of regional extreme cold events (Earlier)



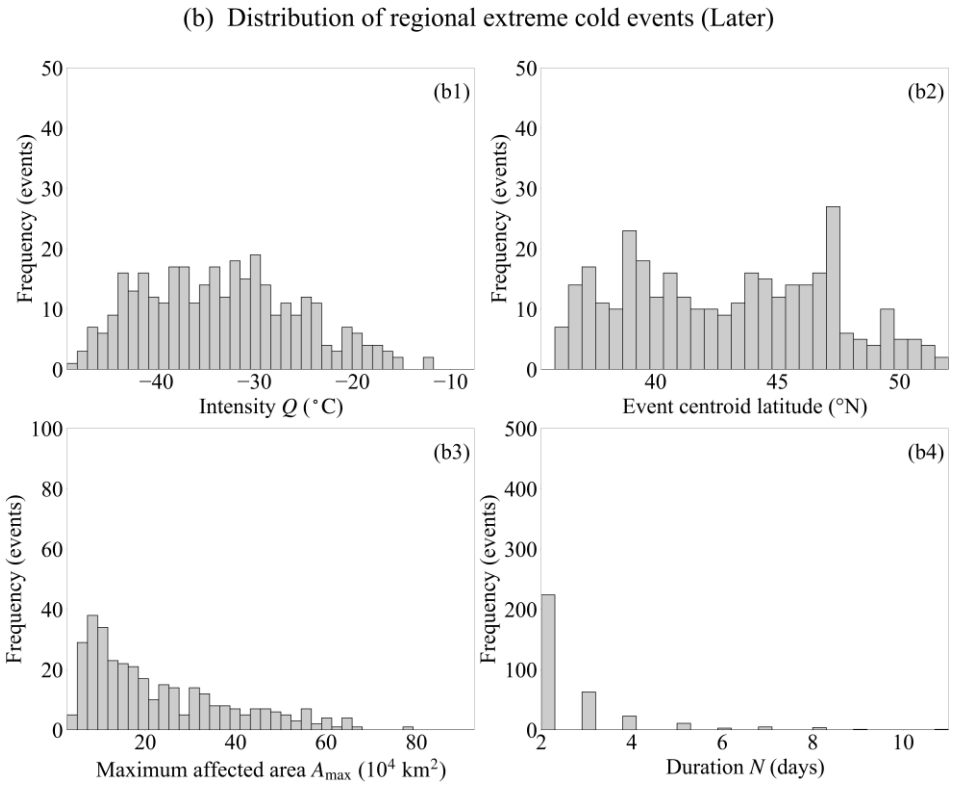


Figure 4. The frequency distribution and differences in regional extreme cold event characteristics before and after the Arctic amplification (AA) in northern China. (**a**) The frequency distribution of the event characteristics of the period before the occurrence of AA. (**b**) The frequency distribution of the period after the occurrence of AA. Specifically, (a1, b1) represent minimum event temperature *(Q)*; (a2, b2) represent event centroid latitude; (a3, b3) represent maximum affected area (Amax); and (a4, b4) represent event duration *(N)*.

The frequency distribution of the lowest temperature *Q* of the event (Figure 4(a1,b1)) showed broad unimodal characteristics in both periods, mainly in the range of −40 to −25 °C, and the peak frequency appeared around −30 °C. Compared with the earlier period, the *Q* distribution in the later period shifted to the low-temperature direction, showing an increase in the frequency of events in the low-temperature range (about −45 to −35 °C), while the frequency of relatively warm events decreased. The distribution of the latitude of the center of the event (Figure 4(a2,b2)) shows multi-peak characteristics, and the center of the event is mainly distributed between 37° and 48° north latitude. Relatively high-frequency regions occur at 38–40° and 45–48° north latitudes, indicating that regional extreme cold events have obvious latitude aggregation. This distribution pattern reflects the differences in the background of cold air activity and climatic conditions in different latitudes in northern China.

The distribution of the maximum impact area (A_max) (Figure 4(a3,b3)) shows significant right-skewed characteristics; that is, as the impact area increases, the event frequency decreases rapidly. Small-area events dominate, while large-scale events are relatively rare. This shows that although regional extreme cold events have a certain spatial continuity, events with a wide range of impact are still low-probability events. The distribution of A_max remains basically the same in the two periods before and after. The duration *(N)* distribution (Figure 4(a4,b4)) also shows significant right-bias features, and the frequency of events decreases rapidly with the extension of duration. Most regional extreme cold events are concentrated in the short duration of 2–3 days, while long duration events occur less frequently. Compared with the early period, the duration distribution of the later period shows a certain adjustment.

Figure 5a further shows that compared with the early stage, the frequency of cold events in the later stage has generally increased (the average difference is −2.98), and the difference has passed the significance test. This shows that the intensity distribution of extreme cold events in the later period has changed significantly, showing the characteristics of increasing extreme low-temperature intensity. Figure 5b shows that the average mass center latitude in the later period moved 0.87° north, and the difference passed the significance test. This indicates that in the later AA period, the activity center of regional extreme cold events shifted to high latitudes. Figure 5c shows that the mean difference between the two periods is −1.63, and the Bootstrap test does not reach the statistical significance level, indicating that the spatial scale of regional extreme cold events has not changed substantially between the two periods. Figure 5d shows that the average frequency difference is +0.18 days, and the difference has passed the significance test, indicating that the frequency distribution between different duration categories has changed to a certain extent; that is, the proportion of relatively long-lasting events in the later stage has increased. However, combined with the results of the average duration in Figure 4a, the average duration of the event has not changed significantly; this shows that the adjustment of the duration distribution mainly reflects the redistribution of the proportion of the event between different duration categories, rather than the systematic extension of the overall duration of the event.

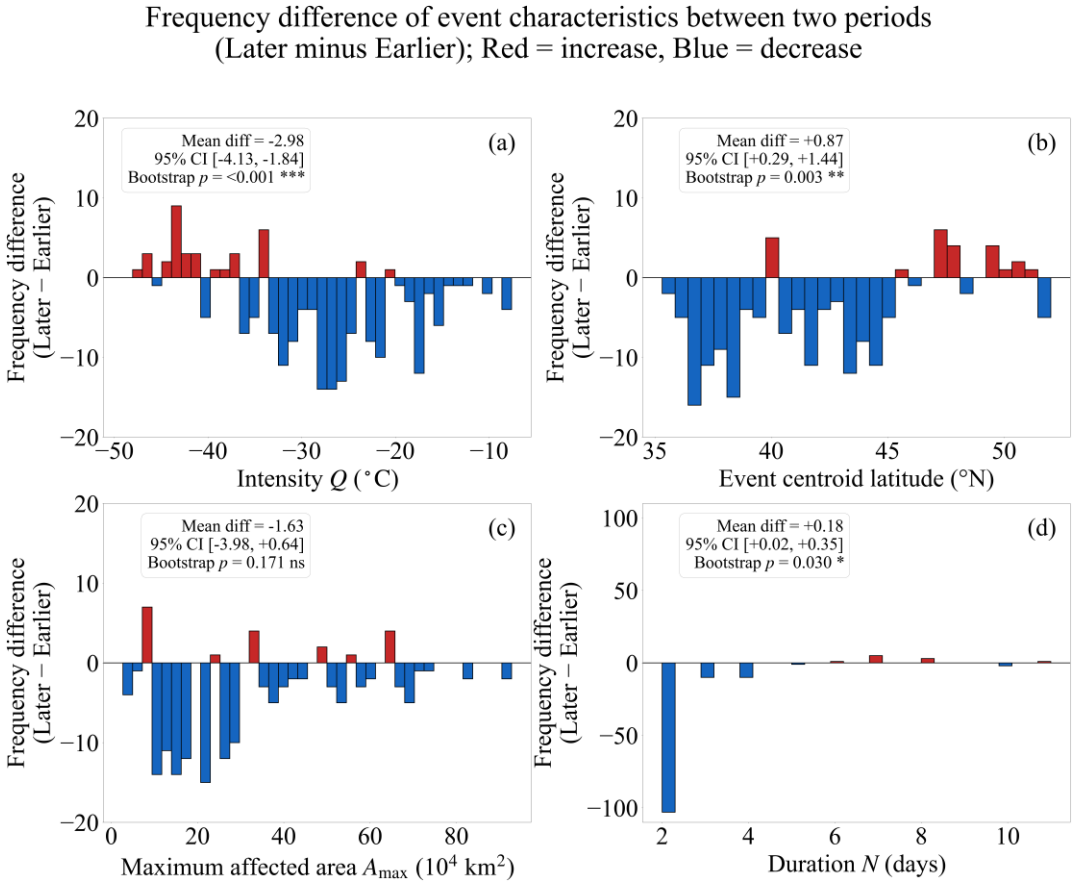


Figure 5. The frequency differences in regional extreme cold event characteristics before and after the Arctic amplification (AA) in northern China. The difference in the frequency distribution of the period after the occurrence of AA and before the occurrence of AA (the latter minus the former). Specifically, (**a**) represent minimum event temperature *(Q)*; (**b**) represent event centroid latitude; (**c**) represent maximum affected area (Amax); and (**d**) represent event duration *(N)*. The red and blue columns indicate the increase and decrease in the frequency of events, respectively. The picture provides the average difference, the Bootstrap 95% confidence interval and the Bootstrap *p*-value to

evaluate the significance of the distribution change. The ns indicates that the trend is not significant ($p \geq 0.05$), while *, ** and *** indicate significance at the levels of $p < 0.05$, $p < 0.01$ and $p < 0.001$, respectively.

In general, regional extreme cold events show non-uniform distribution characteristics in various attributes, among which *Q*, the latitude of the center of mass of the event, A_max and *N*, respectively characterize the differences in thermal intensity, spatial position, scope of influence and duration characteristics. Compared with the previous period, the attribute distribution of regional extreme cold events has shown a certain adjustment. Specifically, in the later stage, the distribution of the lowest temperature of the event shifted to a lower value, the center of the event moved to high latitudes, and the distribution of the duration category changed to a certain extent, while the maximum impact range was not significantly adjusted. In summary, in the later stage of significant Arctic amplification, the changes in regional extreme cold events are mainly manifested in the enhancement of low-temperature intensity, the shift of the event position, and the adjustment of the duration distribution, rather than the systematic expansion of the impact range.

In order to explore the changing characteristics of regional extreme cold events in northern China during different Arctic amplification (AA) periods, this study compares the early and late periods (Earlier period and Later period) from multiple aspects such as event frequency, extreme intensity, duration, scope of influence and spatial distribution. Period) regional extreme cold event (Figure 6).

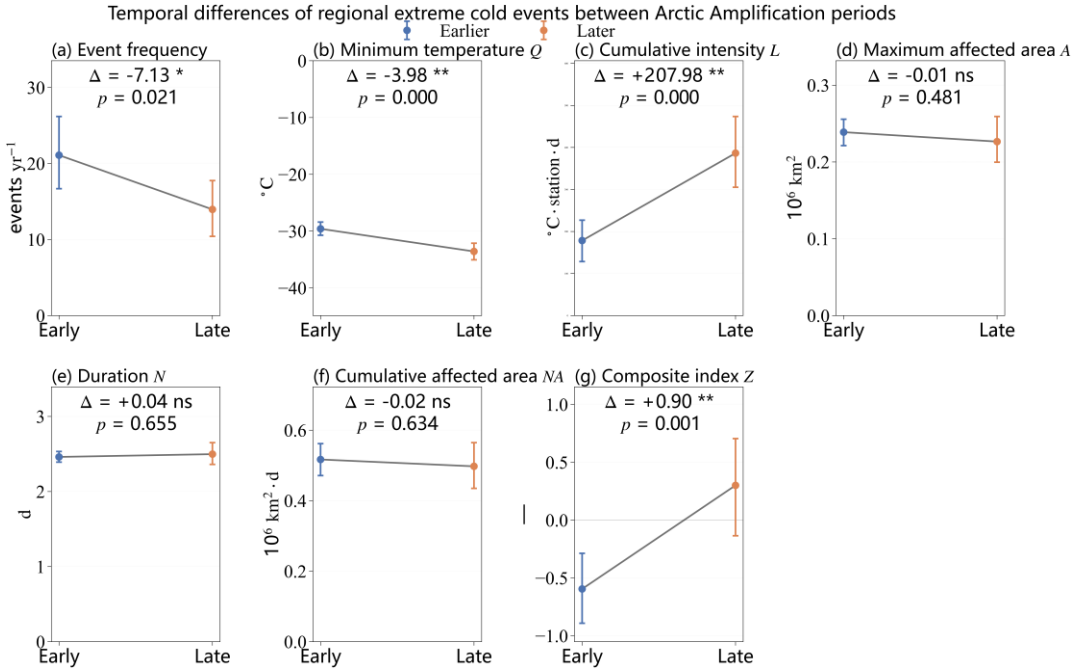


Figure 6. Time changes of regional extreme cold events in northern China during different Arctic amplification periods. The comparison of the characteristics of regional extreme cold events in the early and late stages of the Arctic, including (**a**) event frequency, (**b**) minimum temperature *(Q)*, (**c**) cumulative intensity *(L)*, (**d**) maximum impact area (A), (**e**) duration *(N)*, (**f**) cumulative impact area *(NA)* and (**g**) composite index *(Z)*. The error bar represents the 95% confidence interval obtained by Bootstrap resampling. Δ indicates the difference between the later stage and the early stage. The statistical significance is evaluated by the Bootstrap double-sample significance test. The ns indicates that the trend is not significant ($p \geq 0.05$), while *and ** indicate significance at the levels of $p < 0.05$ and $p < 0.01$, respectively.

Figure 6 shows the differences in the indicators of regional extreme cold events in the two periods. First of all, the frequency of later events decreased significantly (Figure 6a). The average frequency of regional extreme cold events decreased from about 21 times/year in the early stage to about 14 times/year in the later stage, with a change of −7.13 times/year, and the change passed the significance test. The results show that in the late stage of Arctic amplification, the frequency of regional extreme cold events in northern China decreased significantly.

However, in contrast to the decrease in the frequency of events, the indicators related to the intensity of extreme cold events show a significant increasing trend. The minimum temperature indicator Q decreased further in the later stage, from about −29.5 °C in the early period to about −33.5 °C, with a change of −3.98 °C (Figure 6b); the cumulative intensity index L increased significantly, with a change of +207.98 °C·station·day (Figure 6c). Both intensity indicators passed the significance test, indicating that the later extreme cold event has a lower extreme temperature and a stronger cumulative cold anomaly intensity. The comprehensive index Z constructed by multiple indicators further confirms this change: the Z value rises from about −0.6 in the early stage to about 0.3 in the later stage; the change is +0.90 (Figure 6g), and the change passes the significance test. This shows that in terms of overall intensity, regional extreme cold events show an increasing trend in the later stage.

In contrast, indicators related to event lifecycle and spatial scale did not show significant changes. The maximum affected area A changed by only -0.01×10^6 km^2 (Figure 6d), the event duration N changed by +0.04 d (Figure 6e), and the cumulative affected area NA changed by -0.02×10^6 km^2·d (Figure 6f). None of these indicators passed the significance test. These results indicate that the enhanced intensity of extreme cold events during the later period was not caused by prolonged event duration or expanded affected area, but mainly resulted from stronger cold anomalies during individual events.

Therefore, from the temporal perspective, regional extreme cold events over Northern China exhibited a clear shift in their overall characteristics during the later AA period, shifting from relatively high-frequency and relatively weaker cold anomaly events during the earlier period to relatively low-frequency and relatively high-intensity cold anomaly events during the later period.

Figure 7 further shows the spatial distribution and differences in regional extreme cold events in different regions of northern China in two periods. In the previous period (Figure 7a), the high incidence areas of regional extreme cold events were mainly distributed in northeast China, eastern Inner Mongolia and northern North China. Among them, the northeast region presents the most prominent high-value centers, especially in southern Heilongjiang, Jilin and northern Liaoning. These areas have high latitudes, a prominent cold background in winter, and are deeply affected by cold air activity at mid- and high latitudes, resulting in a high frequency of extreme cold events. In addition, from eastern Inner Mongolia to northern North China, there is also a high frequency of events, reflecting the important impact of cold air activity on the Mongolian plateau on regional extreme cold events in northern China.

https://doi.org/10.3390/atmos17111097

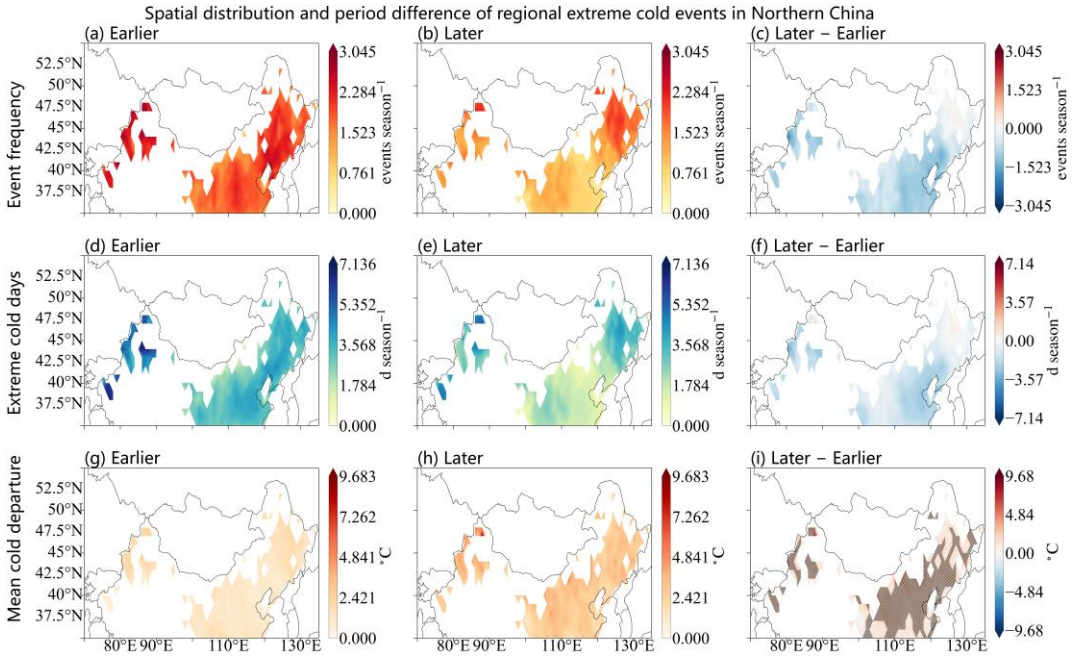


Figure 7. Spatial distribution of regional extreme cold events in northern China during different Arctic amplification periods. Spatial distribution and period differences in regional extreme cold events in northern China. The first line (**a–c**) shows the frequency of events, the second line (**d–f**) shows the number of extremely cold days, and the third line (**g–i**) shows the mean cold anomaly. The first, second and third columns represent the difference between the early stage, the late stage and the late stage minus the early stage, respectively. The difference chart shows the changes in the later period relative to the early stage. Blue and red indicate decrease and increase, respectively. (The shaded area in (**i**)) indicates that the change in the mean cold anomaly level in the later and early stages passed the grid point of the Bootstrap double sample significance test (corrected by Benjamini–Hochberg false discovery rate [FDR]).

In the later period (Figure 7b), the spatial distribution pattern of the frequency of events remained generally stable. The high-frequency zone is still mainly located in the area of "Northeast—Eastern Inner Mongolia—Northern North China", but the overall intensity has weakened. The distribution of the difference between the later period and the previous period (Figure 7c) shows that most areas show negative anomalies, indicating that the frequency of extreme cold events in the later period has generally decreased. This downward trend is particularly obvious in the south-central part of the northeast, eastern North China and eastern Inner Mongolia, which is consistent with the overall downward trend of the frequency of events shown in Figure 6.

The spatial distribution of the number of extreme cold days broadly corresponds to the spatial pattern of event frequency (Figure 7a–f). In the previous period (Figure 7d), the areas with more extreme cold days were mainly concentrated in Northeast China and eastern Inner Mongolia, overlapping with the major high-frequency areas of extreme cold events shown in Figure 7a. This spatial correspondence indicates that the two indicators share similar spatial patterns in these regions. In the later period (Figure 7e), the spatial distribution pattern of extreme cold days remained broadly stable, although the overall number of extreme cold days decreased. The difference map (later minus earlier; Figure 7f) shows predominantly negative anomalies across the study area, indicating a general reduction in the number of extreme cold days. This result is consistent with the overall decrease in event frequency shown in Figure 7c. However, the consistency between the two indicators does not necessarily mean that their spatial distributions or changes are identical at every location.

Unlike the frequency of events and the number of days of extreme cold, the average low temperature abnormality shows an increasing trend (Figure 7g–i). The average low temperature anomaly reflects the deviation of the lowest temperature relative to the threshold temperature during extreme cold events. The higher the value, the stronger the degree of low temperature anomaly. In the early stage (Figure 7g), strong low-temperature abnormalities were mainly distributed in Northeast China, eastern Inner Mongolia and northern North China, which is consistent with the high-incidence areas of extreme cold events; this indicates that the above-mentioned areas are not only areas with frequent extreme cold events, but also areas with a strong degree of low-temperature abnormalities. In the later stage (Figure 7h), the average low temperature abnormality increased as a whole, especially in Northeast China, eastern Inner Mongolia and central and eastern North China. The results of the difference between the late stage and the early stage (Figure 7i) show that most areas show positive abnormalities, and some areas have passed the significance test, indicating that the extreme cold event in the later stage shows a more significant temperature deviation. The areas with significant enhancement are mainly concentrated in Northeast China, eastern Inner Mongolia and central and eastern North China, which implies that the enhancement of late extreme cold events in these areas is statistically significant and not caused by random interannual changes.

By combining the temporal variations and spatial distributions, it can be found that regional extreme cold events over Northern China during the later AA period did not exhibit a simple enhancement or weakening pattern but instead showed clear asynchronous changes.

On the one hand, the frequency of a wide range of events and the number of days of extreme cold in the research area have decreased, indicating that the frequency of regional extreme cold events has decreased; on the other hand, the minimum temperature, the cumulative low temperature intensity and the average low temperature abnormality have all increased significantly, showing that the extreme cold events that occur in the later stage show stronger low-temperature abnormal characteristics.

In terms of spatial distribution, Northeast China, eastern Inner Mongolia and northern North China are still key areas affected by regional extreme cold events. However, the areas with increased intensity in the later stage are mainly concentrated in Northeast China and central and eastern North China, and some areas have passed the significance test. In general, during the later AA period, the regional extreme cold events in northern China showed the characteristics of "reducing the frequency of events, but increasing the abnormal intensity of the low temperature of a single event".

3.2. Relationships Between Arctic Amplification, Key Circulation Anomalies, and Regional Extreme Cold Events

To further explore the relationship between extreme cold events in northern China and key circulation anomalies under Arctic amplification (AA), this study constructed the Arctic amplification index (AAI850), the Siberian High Index (SHI), and the Ural Ridge Index (URI), and analyzed their interannual changes and correlations with regional extreme cold event indices (Figure 8). Here, AAI850 characterizes Arctic warming relative to mid-latitudes, whereas SHI and URI depict near-surface pressure anomalies over the Siberian–Mongolian region and 500 hPa geopotential height anomalies over the Ural region, respectively.

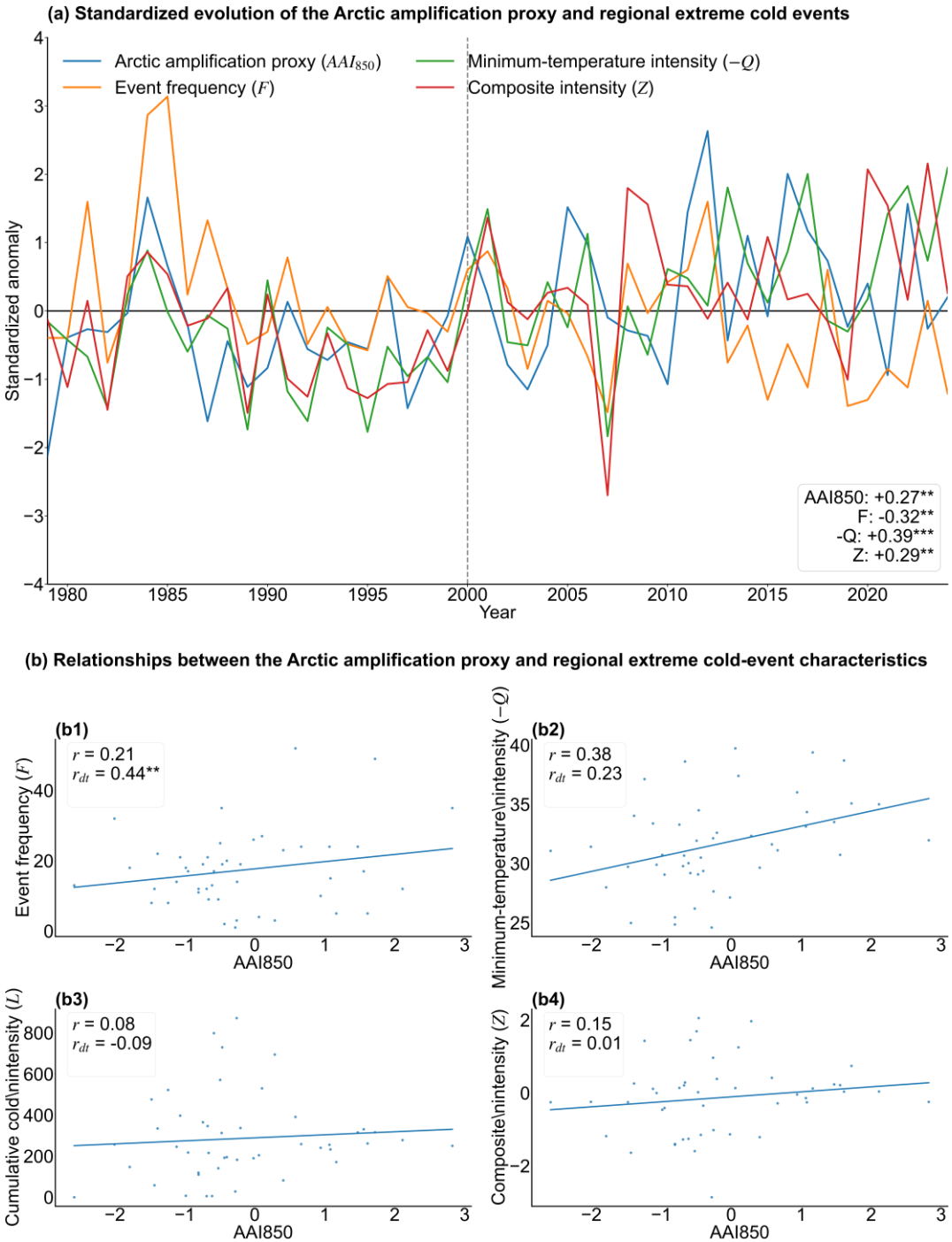


Figure 8. The statistical relationship between the Arctic amplification index and the characteristics of regional extreme cold events in northern China. (**a**) Standardized interannual changes between AAI850 and regional extreme cold event index from 1979 to 2024, including Arctic amplification index (AAI850), event frequency (F), minimum temperature cold intensity (−*Q*) and composite intensity index *(Z)*. The solid line represents the linear trend, and the trend significance is evaluated by the residual moving-block bootstrap method. (**b**) The correlation between AAI850 and various regional extreme cold event indices: (b1) event frequency (F); (b2) minimum-temperature cold intensity (−*Q*); (b3) cumulative cold intensity *(L)*; and (b4) composite intensity index *(Z)*. Each dot represents an annual observation, and the solid line indicates the linear regression fit. The figure shows the Pearson correlation coefficient of the original sequence and the detrended time series, and the significance is evaluated by the Bootstrap method. While **and *** indicate significance at the levels of $p < 0.01$ and $p < 0.001$, respectively.

Figure 8a shows the standardized interannual variations in AAI850 and the regional extreme cold-event indices from 1979 to 2024. During the study period, AAI850 exhibits a statistically significant upward trend, indicating enhanced Arctic warming relative to the midlatitudes. Meanwhile, regional extreme cold-event frequency (F) shows a significant downward trend, whereas minimum-temperature intensity (−*Q*) and composite intensity *(Z)* exhibit significant upward trends. All four trends are statistically significant according to the bootstrap test. These results indicate that strengthening Arctic amplification coincides with decreasing event frequency and increasing intensity as measured by −*Q* and Z in northern China. This pattern is consistent with the transition from more frequent, weaker events to less frequent, stronger events across the Arctic amplification periods identified in Figure 4. However, these concurrent long-term changes alone do not establish a causal relationship.

Figure 8b further illustrates the correlations between AAI850 and the different regional extreme cold-event indices. Pearson correlation coefficients were calculated for both the original and detrended time series, and their statistical significance was assessed using a bootstrap method. For event frequency F (Figure 8(b1)), the correlation with AAI850 is weak and statistically insignificant in the original time series, but becomes stronger and statistically significant after detrending. This indicates a positive association between their interannual variations after the long-term trends are removed.

For minimum-temperature intensity −*Q* (Figure 8(b2)), the correlations with AAI850 are positive in both the original and detrended time series, but neither is statistically significant. Thus, although −*Q* exhibits a significant upward trend in Figure 8a, the correlation analysis does not establish a significant linear association between its interannual variability and AAI850. For cumulative cold intensity *L* (Figure 8(b3)) and composite intensity Z (Figure 8(b4)), the correlations with AAI850 are also statistically insignificant. The corresponding coefficients for the original and detrended time series are 0.08 and −0.09 for *L*, and 0.15 and 0.01 for Z, respectively. These results provide no statistically significant evidence of linear associations between AAI850 and these two indices over the study period.

Taken together, Figure 8a,b highlight the distinction between long-term changes and detrended interannual relationships. Over 1979–2024, AAI850 increases while event frequency decreases and the −*Q* and Z intensity indices increase. After detrending, however, AAI850 exhibits a significant positive correlation with event frequency, whereas its correlations with all three intensity indices remain statistically insignificant. Thus, the opposing long-term trends in AAI850 and event frequency coexist with positive interannual covariability. These results emphasize that relationships between Arctic amplification and regional extreme cold events depend on the temporal component examined, and that concurrent long-term trends should be distinguished from interannual associations.

Figure 9 shows the detrended correlation between AAI850, SHI, URI, and regional extreme cold event indices. All correlation coefficients are calculated based on the detrended time series, and the significance test is carried out by the Bootstrap method. The results show that there is a significant positive correlation between AAI850 and SHI, indicating that the abnormal changes in the Siberian High are consistent with the change trend of Arctic amplification. AAI850 and URI also have a significant positive correlation, suggesting that there is a synergistic change between Arctic amplification and high-altitude circulation anomalies in the Urals. In addition, there is also a significant correlation between SHI and URI, indicating that there is a certain degree of synchronous variability between the two key circulation anomalies at high latitudes in Eurasia.

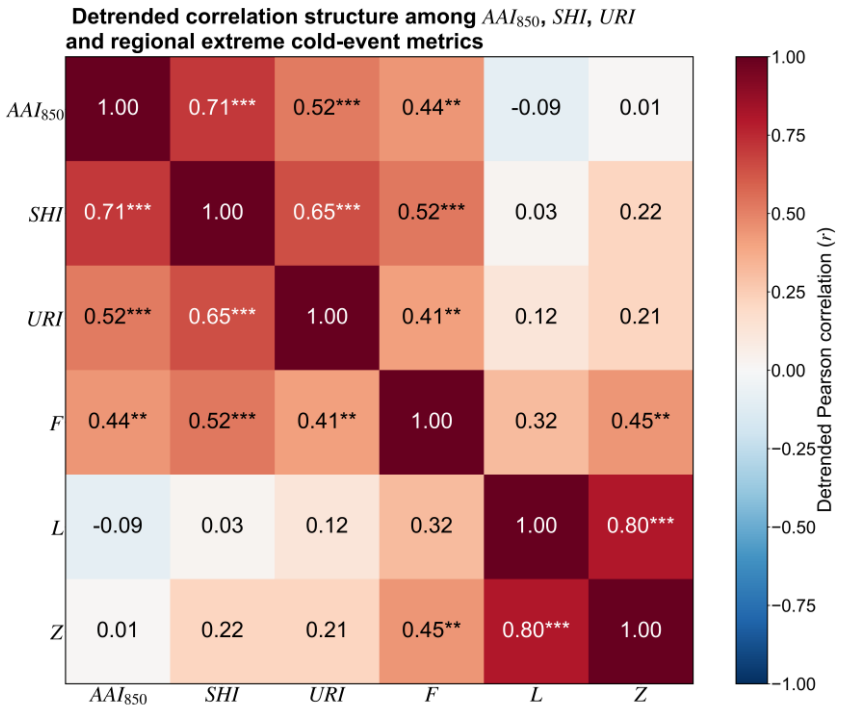
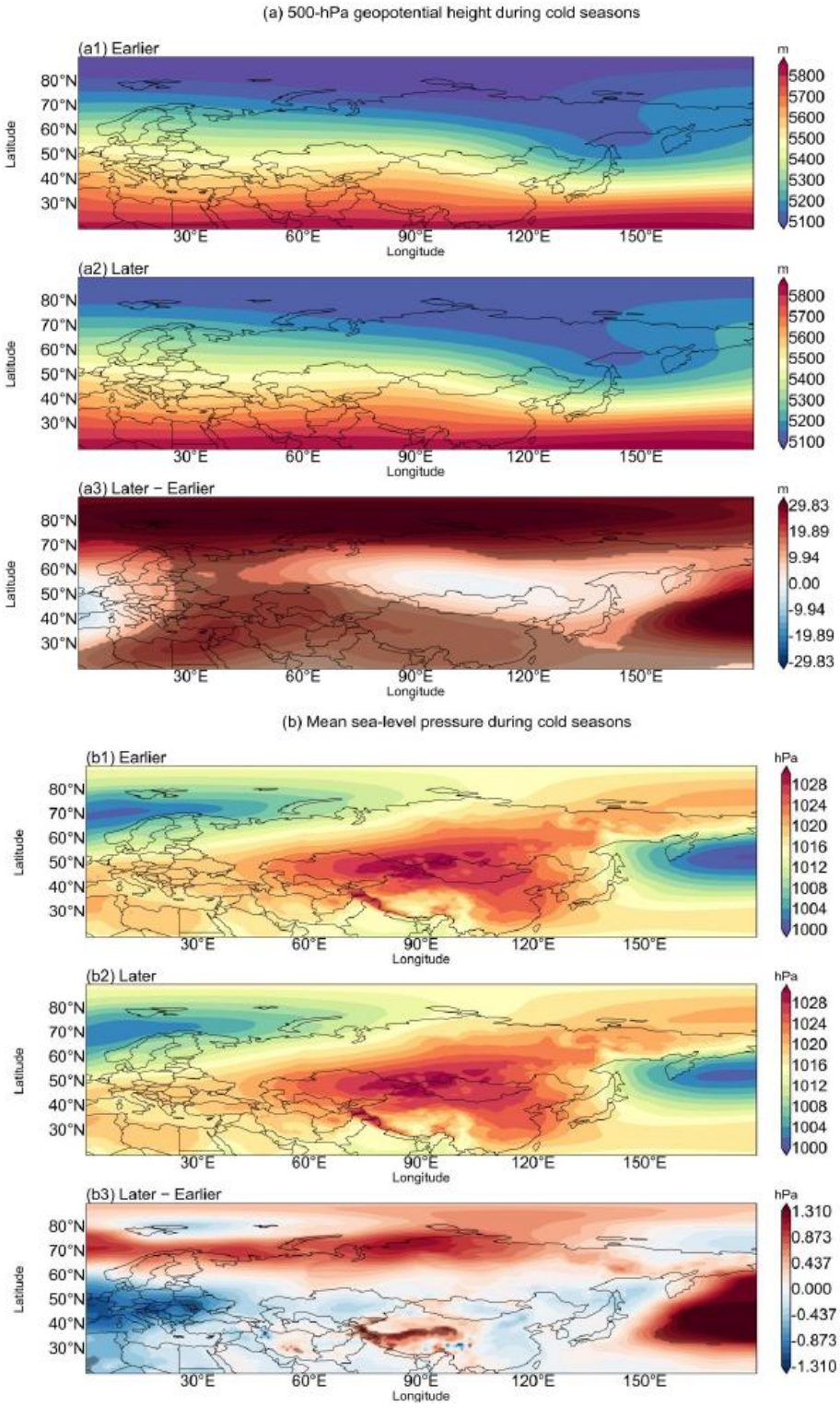


Figure 9. The statistical relationship between the Arctic amplification index, the circulation anomaly index and the characteristics of regional extreme cold events in northern China. The detrended correlation matrix between AAI850, circulation anomaly index (SHI and URI) and regional extreme cold event index. All correlations are calculated based on the detrended time series and tested by the Bootstrap method. ** and *** indicate $p_{boot} < 0.01$ and $p_{boot} < 0.001$, respectively.

Among extreme cold event indices, cumulative cold intensity *L* is significantly positively correlated with the composite intensity index Z, indicating that Z mainly reflects the cumulative characteristics of cold anomalies. At the same time, the circulation anomaly index is positively correlated with the event frequency F, suggesting that there is a statistical correlation between the high-latitude circulation anomaly in Eurasia and the occurrence characteristics of regional extreme cold events.

Taken together, Figure 8a,b distinguish long-term changes from relationships between the detrended time series. Over 1979–2024, AAI850 exhibits a significant upward trend, while event frequency shows a significant downward trend and the −*Q* and Z intensity indices show significant upward trends. After detrending, AAI850 is significantly positively correlated with event frequency, whereas its correlations with all three intensity indices are statistically insignificant. Thus, the opposing long-term trends in AAI850 and event frequency coexist with significant positive covariability in their detrended variations. These findings underscore the need to distinguish concurrent long-term changes from correlations between detrended variations when interpreting the associations between AAI850 and regional extreme cold-event characteristics.

To further understand differences in regional extreme cold events over northern China under different Arctic amplification (AA) periods, this study examined the large-scale circulation background during extreme cold events, including 500 hPa geopotential height, sea level pressure, and 850 hPa temperature, geopotential height, and wind fields (Figure 10).



https://doi.org/10.3390/atmos17111097

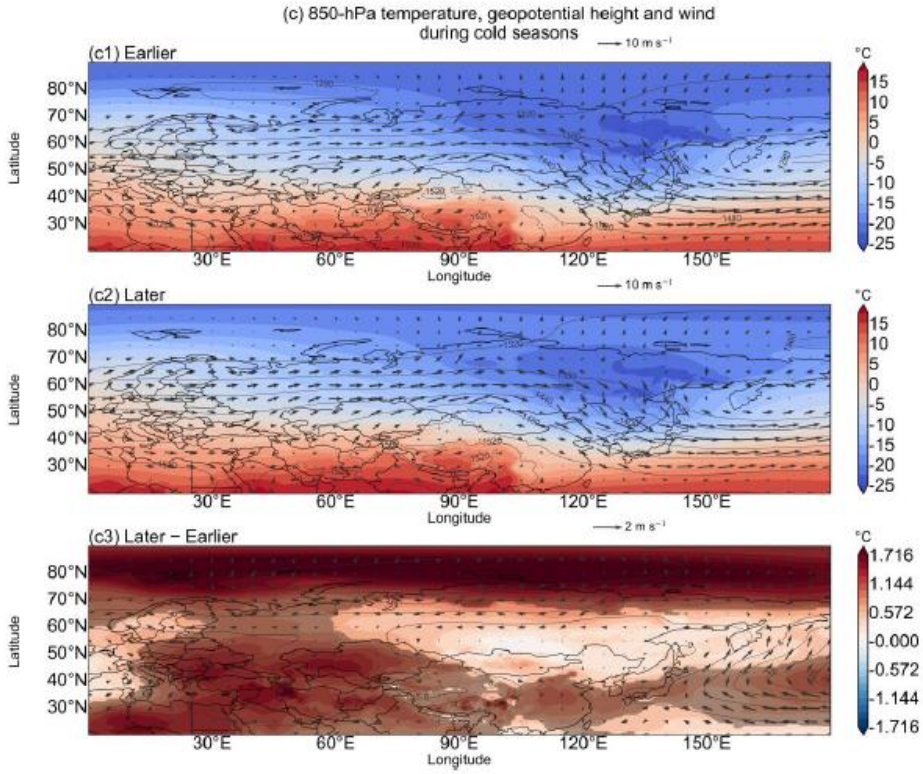


Figure 10. Characteristics of atmospheric circulation synthesis during regional extreme cold events in northern China during different Arctic amplification periods. (**a**) Composite diagram of the 500 hPa potential height field during regional extreme cold events: early stage (**a1**), late stage (**a2**) and the difference between the two (late stage minus early stage) (**a3**). (**b**) Synthesis diagram of sea-level pressure field during regional extreme cold events: early (**b1**), late (**b2**) and the difference between the two (late minus early) (**b3**). (**c**) Composite diagram of 850 hPa temperature, potential height and wind field during regional extreme cold events: early stage (**c1**), late stage (**c2**) and the difference between the two (late stage minus early stage) (**c3**). The shaded area represents 850 hPa temperature in (**c1**,**c2**), and the temperature difference in (**c3**); the equivalent line represents the 850 hPa potential height; the vector arrow represents the horizontal wind field. The shaded slash area in the difference chart represents the area where the change is statistically significant at the 95% confidence level.

The 500 hPa geopotential height field characterizes the large-scale mid-tropospheric circulation during cold seasons. In the earlier period (Figure 10(a1)), geopotential height generally decreases with increasing latitude across Eurasia, with lower values at high latitudes and higher values at middle and lower latitudes. Northern China lies within this pronounced meridional geopotential height gradient. In the later period (Figure 10(a2)), the broad spatial pattern remains similar, while regional changes become evident in the later-minus-earlier difference field. Figure 10(a3) shows predominantly positive geopotential height differences across the plotted domain. Widespread statistically significant increases occur over the Arctic and northern Eurasia, as well as across substantial parts of lower- to midlatitude Eurasia, including parts of China, and the western North Pacific. In contrast, a band extending through parts of central and eastern Eurasia around 45–60° N exhibits comparatively small differences that are generally statistically insignificant. Localized weak negative differences also occur within this band and over parts of western Europe. These results indicate widespread but spatially nonuniform increase in cold-season 500 hPa geopotential height, rather than an adjustment confined mainly to high latitudes.

The mean sea-level pressure field reflects the characteristics of the large-scale near-surface pressure system during cold seasons. In the earlier period (Figure 10(b1)), a

pronounced continental high-pressure system extends across interior Eurasia, with high sea-level pressure over the Siberian–Mongolian region. Northern China lies along the southern to southeastern flank of this high-pressure system. In the later period (Figure 10(b2)), high pressure persists over the Siberian–Mongolian region, and the broad spatial pattern remains similar to that of the earlier period. The later-minus-earlier difference field (Figure 10(b3)) shows a broad band of positive sea-level pressure differences across northern Eurasia, although much of this band does not reach statistical significance. Significant positive differences occur over parts of the Tibetan Plateau and a broad area of the western North Pacific, while significant negative differences occur in parts of Europe. Over much of northern China outside the Tibetan Plateau, the differences are comparatively small and generally statistically insignificant. These results indicate that the broad continental high-pressure pattern persists between the two periods, while changes in cold-season mean sea-level pressure exhibit marked regional differences rather than being confined to high latitudes.

The temperature, geopotential height, and wind fields at the 850 hPa pressure level characterize the lower-tropospheric thermal and circulation conditions during cold seasons. In the earlier period (Figure 10(c1)), relatively cold conditions prevail over northeastern China and eastern Inner Mongolia, with temperatures generally decreasing northward. The wind field exhibits northwesterly or northerly components over parts of northern China, consistent with the potential for southward transport of colder air. In the later period (Figure 10(c2)), the broad spatial patterns of temperature, geopotential height, and wind remain similar to those in the earlier period. The later-minus-earlier difference field (Figure 10(c3)) shows predominantly positive temperature differences, with statistically significant warming indicated by hatching across extensive high-latitude areas and substantial parts of lower- to midlatitude Eurasia, including parts of China. In contrast, portions of central and eastern Siberia exhibit comparatively small temperature differences that generally do not reach statistical significance. These results indicate a generally warmer cold-season lower-tropospheric background in the later period. The geopotential height contours and wind vectors also exhibit regional differences between the two periods. Northwesterly or northerly wind components remain evident over parts of northern China in the later-period mean field. The persistence of northwesterly or northerly wind components over parts of northern China is consistent with the possibility of continued southward cold-air transport in the later period. Thus, despite the warmer cold-season thermal background, the mean circulation retains features potentially conducive to cold-air incursions into northern China.

Taken together, the circulation fields at different levels in Figure 10 reveal changes in the cold-season thermal and circulation background between the earlier and later periods. At 500 hPa, geopotential height increases over extensive areas of the Arctic and Eurasia, with substantial regional differences in the magnitude and statistical significance of these changes. The spatially nonuniform increase may modify regional height gradients and the background flow that steers cold air, potentially affecting its southward pathways into northern China. At sea level, the broad Siberian–Mongolian high-pressure pattern persists in both periods, while significant pressure differences occur in selected regions rather than indicating a uniform strengthening of the continental high. These regional pressure changes may alter pressure gradients and low-level flow patterns, potentially influencing the pathways and strength of cold-air transport into northern China. At 850 hPa, predominantly positive temperature differences indicate a warmer lower-tropospheric background in the later AA period. Nevertheless, northwesterly or northerly wind components remain evident over parts of northern China, consistent with the possibility of southward cold-air transport. Thus, the later period combines a warmer seasonal-mean thermal background with circulation features that may still permit cold-air incursions.

These background changes provide context for the reduced frequency and enhanced cold-anomaly intensity of regional extreme cold events reported in Figure 6.

4. Discussion

This study systematically examines changes in regional extreme cold events over northern China under Arctic amplification using long-term station observations and reanalysis data. From the perspectives of event characteristics, statistical relationships, and large-scale circulation backgrounds, the results show that Arctic amplification is associated with reduced event frequency and enhanced cold intensity. Circulation composites further suggest that residual extreme cold events occur under specific mid- and high-latitude configurations. Given regional differences in the response of midlatitude climate to Arctic amplification, future work should expand the domain and compare response characteristics across regions.

Compared with previous observational and modeling studies, the present results emphasize that regional extreme cold events over northern China did not disappear under Arctic amplification; instead, their statistical structure changed from high-frequency/weak-anomaly events to low-frequency/high-intensity events [14,16–21]. This is consistent with arguments that warming reduces the frequency of threshold-exceeding cold processes, whereas residual events remain controlled by strong circulation anomalies such as Siberian High intensification and Ural blocking [20,22,24,25].

By jointly examining changes in the frequency, intensity, and circulation background of regional extreme cold events over northern China, this study provides regional observational evidence for understanding the relationship between Arctic amplification (AA) and midlatitude cold extremes. The identified transition from more frequent, weaker-anomaly events to less frequent, stronger-anomaly events also offers a regional perspective on the evolution of cold extremes under Arctic warming. Existing studies provide different interpretations of the midlatitude impacts of AA. Cohen et al. identified associations between anomalous Arctic warmth and severe winter weather over Northern Hemisphere continents [50]. Other studies place greater emphasis on natural climate variability in shaping the warm Arctic–cold Eurasia pattern. Zhou et al. found that winter cooling over central Eurasia was mainly associated with enhanced cold-air advection driven by Ural blocking, highlighting the roles of internal atmospheric variability and the North Atlantic Oscillation [51]. Furthermore, Ku et al. distinguished the contributions of AA and internal circulation variability to this pattern, finding that AA contributed to Arctic warming during 1990–2014, whereas the negative phase of the Arctic Oscillation contributed to Eurasian cooling, while also emphasizing interactions between these components [52]. ENSO may also influence East Asian winter climate and the circulation background associated with cold events. Geng et al. showed that ENSO impacts on East Asian winter climate vary within the season, including a temporary breakdown in mid-January associated with changes in North Atlantic circulation [53]. Cold-season averages may therefore obscure subseasonal differences in ENSO influences. Although these studies differ in geographical coverage, temporal scales, and diagnostic measures, they collectively highlight the need to consider Arctic influences alongside natural climate variability. The frequency and intensity changes identified here cannot yet be attributed exclusively to AA, as internal atmospheric variability and other factors, including ENSO, may also contribute. Building on the regional observational evidence established here, future research could undertake targeted attribution analyses to further clarify the relative contributions of AA and other climate processes.

Background warming and individual cold outbreaks describe different aspects of climate variability. A warmer seasonal mean does not eliminate transient circulation configurations capable of transporting colder air southward. Blocking and amplified

trough–ridge patterns can favor meridional flow, while continental high-pressure systems can support cold-air accumulation and subsequent southward movement [20,22,24,25]. In Figure 10, northwesterly or northerly wind components remain evident over parts of northern China at 850 hPa despite the warmer thermal background. Spatially nonuniform changes in geopotential height and sea-level pressure may further modify the background flow and transport pathways. These features are consistent with the possibility of southward cold-air transport, but do not determine whether transport has strengthened or weakened. These features provide a possible physical context for the persistence of cold outbreaks. One hypothesis is that events producing pronounced cold anomalies in the later period involve particularly favorable circulation configurations for cold-air transport and accumulation. Future work could test this hypothesis using event-based circulation composites, temperature-advection diagnostics, and analyses of circulation persistence.

The present correlation analysis does not, by itself, establish that Arctic amplification caused the observed changes in extreme cold events. Alternative drivers cannot be excluded, including the Arctic Oscillation/North Atlantic Oscillation, El Niño–Southern Oscillation, volcanic forcing, and changes in station siting or urban heat-island effects on station minimum temperature. Future work should therefore combine observational attribution, coupled model experiments, and station homogenization tests.

Several methodological limitations should be noted. First, AAI850 is only one of many Arctic amplification metrics, and conclusions may be sensitive to the chosen latitude bands. Second, the period division around 2000 is a comparative framework rather than a unique physical transition. Third, regional event detection depends on thresholds and spatial–temporal continuity criteria that may bias frequency trends if station density or quality changes over time. Fourth, composite circulation maps describe mean states and do not quantify causal pathways or predictability.

Future work will also assess how station latitude, elevation and spatial distribution influence the results through sensitivity analyses, alongside event-based diagnostics of cold-air transport and analyses of other climate drivers.

In terms of practical implications, the shift toward fewer but more intense regional extreme cold events suggests that risk assessment for northern China should emphasize intensity and concurrent multi-region cold-air outbreaks rather than event counts alone. Because the maximum affected area and mean duration show no robust changes in this dataset, design standards that depend mainly on exposure duration may need complementary information from other event types.

Finally, these results support the view that the Arctic–midlatitude linkage is region-dependent and asymmetric [14–19,21]. Extending the analysis to other Eurasian sectors and to subseasonal-to-seasonal prediction frameworks would help determine whether the frequency–intensity decoupling identified here is a general feature of midlatitude extreme cold events under Arctic amplification.

5. Conclusions

This study identified extreme cold events in northern China for the cold seasons of 1979/80–2023/24 using the Arctic amplification index (AAI850), Siberian High Index (SHI), Ural Ridge Index (URI), and atmospheric circulation data to examine their changes and associated circulation characteristics under different Arctic amplification (AA) periods. The main conclusions are as follows:

During the research period, AAI850 showed a significant upward trend, while the frequency of regional extreme cold events decreased significantly, and the low-temperature intensity and composite intensity of the lowest temperature were significantly enhanced. Compared with the earlier AA period, extreme cold events in the later period shift from a “high-frequency, weak-anomaly” state to a “low-frequency, high-

intensity" state. During the later AA period, the minimum temperature of extreme cold events shifts toward colder conditions, the event centers move toward higher latitudes, and the duration structure changes, while the affected area shows no significant change. These results indicate that the intensification of extreme cold events is mainly associated with enhanced cold anomalies rather than an expansion of affected areas.

AAI850 shows significant correlations with some extreme cold event indices as well as SHI and URI, suggesting coordinated variations between Arctic amplification and Eurasian mid–high latitude circulation anomalies. During the later AA period, adjustments are observed in the 500 hPa geopotential height field, sea level pressure field, and 850 hPa lower-tropospheric temperature–wind field. Under an overall warmer background, cold air can still influence Northern China through specific circulation configurations, resulting in stronger cold anomalies.

In summary, under the background of Arctic amplification, the extreme cold events in northern China did not show a simple trend of intensification or weakening, but showed an asynchronous response characteristic; that is, the frequency of events decreased, but the intensity of a single event increased. This change is related to the abnormal adjustment of high-latitude circulation in Eurasia.

Supplementary Materials: The following supporting information can be downloaded at: https://www.mdpi.com/article/10.3390/atmos17111097/s1. Table S1: Sensitivity analysis of regional extreme cold event characteristics under alternative temporal boundary definitions.

Author Contributions: Y.Z., data curation, methodology development, and original draft preparation; J.L., research design and methodology development. All authors have read and agreed to the published version of the manuscript.

Funding: This work was jointly supported by the Fundamental Research Funds for the Central Universities (Project: Impacts of the Stratospheric Polar Vortex on Winter Aircraft Icing Events in China under Arctic Amplification) and the Sichuan Provincial Undergraduate Innovation Training Program (No. S202610624079).

Institutional Review Board Statement: Not applicable.

Informed Consent Statement: Not applicable.

Data Availability Statement: Station observations and reanalysis products analyzed in this study are available from the corresponding author upon reasonable request. ERA5 is freely available from the Copernicus Climate Data Store.

Acknowledgments: We would also like to thank the European Centre for Medium-Range Weather Forecasts (ECMWF) for providing the ERA5 dataset.

Conflicts of Interest: The authors declare no conflicts of interest.

References

1. Screen, J.A.; Simmonds, I. The central role of diminishing sea ice in recent Arctic temperature amplification. *Nature* **2010**, *464*, 1334–1337. https://doi.org/10.1038/nature09051.
2. Serreze, M.C.; Barry, R.G. Processes and impacts of Arctic amplification: A research synthesis. *Glob. Planet. Change* **2011**, *77*, 85–96. https://doi.org/10.1016/j.gloplacha.2011.03.004.
3. Rantanen, M.; Karpechko, A.Y.; Lipponen, A.; Nordling, K.; Hyvärinen, O.; Ruosteenoja, K.; Vihma, T.; Laaksonen, A. The Arctic has warmed nearly four times faster than the globe since 1979. *Commun. Earth Environ.* **2022**, *3*, 168. https://doi.org/10.1038/s43247-022-00498-3.
4. Pithan, F.; Mauritsen, T. Arctic amplification dominated by temperature feedbacks in contemporary climate models. *Nat. Geosci.* **2014**, *7*, 181–184. https://doi.org/10.1038/ngeo2071.

5. Dai, A.; Luo, D.; Song, M.; Liu, J. Arctic amplification is caused by sea-ice loss under increasing CO_2. *Nat. Commun.* **2019**, *10*, 121. https://doi.org/10.1038/s41467-018-07954-9.
6. Previdi, M.; Smith, K.L.; Polvani, L.M. Arctic amplification of climate change: A review of underlying mechanisms. *Environ. Res. Lett.* **2021**, *16*, 093003. https://doi.org/10.1088/1748-9326/ac1c29.
7. Davy, R.; Chen, L.; Hanna, E. Arctic amplification metrics. *Int. J. Climatol.* **2018**, *38*, 4384–4394. https://doi.org/10.1002/joc.5675.
8. Cohen, J.; Screen, J.A.; Furtado, J.C.; Barlow, M.; Whittleston, D.; Coumou, D.; Francis, J.; Dethloff, K.; Entekhabi, D.; Overland, J.; et al. Recent Arctic amplification and extreme mid-latitude weather. *Nat. Geosci.* **2014**, *7*, 627–637. https://doi.org/10.1038/ngeo2234.
9. Chylek, P.; Folland, C.; Klett, J.D.; Wang, M.; Hengartner, N.; Lesins, G.; Dubey, M.K. Annual mean Arctic amplification 1970–2020: Observed and simulated by CMIP6 climate models. *Geophys. Res. Lett.* **2022**, *49*, e2022GL099371. https://doi.org/10.1029/2022GL099371.
10. Davy, R.; Griewank, P. Arctic amplification has already peaked. *Environ. Res. Lett.* **2023**, *18*, 084003. https://doi.org/10.1088/1748-9326/ace273.
11. Stroeve, J.C.; Kattsov, V.; Barrett, A.; Serreze, M.; Pavlova, T.; Holland, M.; Meier, W.N. Trends in Arctic sea ice extent from CMIP5, CMIP3 and observations. *Geophys. Res. Lett.* **2012**, *39*, L16502. https://doi.org/10.1029/2012GL052676.
12. Copernicus Climate Change Service. Sea Ice. Climate Indicators. Available online: https://climate.copernicus.eu/climate-indicators/sea-ice (accessed on 2 November 2026).
13. Notz, D.; Stroeve, J. Observed Arctic sea-ice loss directly follows anthropogenic CO_2 emission. *Science* **2016**, *354*, 747–750. https://doi.org/10.1126/science.aag2345.
14. Cohen, J.; Zhang, X.; Francis, J.; Jung, T.; Kwok, R.; Overland, J.; Ballinger, T.J.; Bhatt, U.S.; Chen, H.W.; Coumou, D.; et al. Divergent consensuses on Arctic amplification influence on midlatitude severe winter weather. *Nat. Clim. Change* **2020**, *10*, 20–29. https://doi.org/10.1038/s41558-019-0662-y.
15. Overland, J.E.; Dethloff, K.; Francis, J.A.; Hall, R.J.; Hanna, E.; Kim, S.-J.; Screen, J.A.; Shepherd, T.G.; Vihma, T. Nonlinear response of mid-latitude weather to the changing Arctic. *Nat. Clim. Change* **2016**, *6*, 992–999. https://doi.org/10.1038/nclimate3121.
16. Blackport, R.; Screen, J.A.; van der Wiel, K.; Bintanja, R. Minimal influence of reduced Arctic sea ice on coincident cold winters in mid-latitudes. *Nat. Clim. Change* **2019**, *9*, 697–704. https://doi.org/10.1038/s41558-019-0551-4.
17. Blackport, R.; Screen, J.A. Insignificant effect of Arctic amplification on the amplitude of midlatitude atmospheric waves. *Sci. Adv.* **2020**, *6*, eaay2880. https://doi.org/10.1126/sciadv.aay2880.
18. Kim, G.; Lee, W.-S.; Kim, B.-M. Can seasonal prediction models capture the Arctic mid-latitude teleconnection on monthly time scales? *Atmos. Sci. Lett.* **2024**, *25*, e1235. https://doi.org/10.1002/asl.1235.
19. Screen, J.A.; Simmonds, I. Exploring links between Arctic amplification and mid-latitude weather. *Geophys. Res. Lett.* **2013**, *40*, 959–964. https://doi.org/10.1002/grl.50174.
20. Petoukhov, V.; Semenov, V.A. A link between reduced Barents-Kara sea ice and cold winter extremes over northern continents. *J. Geophys. Res. Atmos.* **2010**, *115*, D21111. https://doi.org/10.1029/2009JD013568.
21. Smith, D.M.; Eade, R.; Andrews, M.B.; Ayres, H.; Clark, A.; Chripko, S.; Deser, C.; Dunstone, N.J.; García-Serrano, J.; Gastineau, G.; et al. Robust but weak winter atmospheric circulation response to future Arctic sea ice loss. *Nat. Commun.* **2022**, *13*, 727. https://doi.org/10.1038/s41467-022-28283-y.
22. Gong, D.Y.; Wang, S.W.; Zhu, J.H. East Asian winter monsoon and Arctic Oscillation. *Geophys. Res. Lett.* **2001**, *28*, 2073–2076. https://doi.org/10.1029/2000GL012311.
23. Jeong, J.H.; Ho, C.H. Changes in occurrence of cold surges over East Asia in association with Arctic Oscillation. *Geophys. Res. Lett.* **2005**, *32*, L14704. https://doi.org/10.1029/2005GL023024.
24. Yao, Y.; Luo, D.; Dai, A.; Simmonds, I. Increased quasi stationarity and persistence of winter Ural blocking and Eurasian extreme cold events in response to Arctic warming. Part I: Insights from observational analyses. *J. Clim.* **2017**, *30*, 3549–3568. https://doi.org/10.1175/JCLI-D-16-0261.1.
25. Luo, D.; Yao, Y.; Dai, A.; Simmonds, I.; Zhong, L. Increased quasi stationarity and persistence of winter Ural blocking and Eurasian extreme cold events in response to Arctic warming. Part II: A theoretical explanation. *J. Clim.* **2017**, *30*, 3569–3587. https://doi.org/10.1175/JCLI-D-16-0262.1.
26. Zhuo, W.; Yao, Y.; Luo, D.; Huang, F.; Luo, B.; Zhong, L. The response of atmospheric blocking and East Asian cold extremes to future Arctic Sea ice loss. *Atmos. Res.* **2024**, *304*, 107355. https://doi.org/10.1016/j.atmosres.2024.107355.

27. Ye, Y.; Qian, C.; Dai, A.; Zhang, Y.; Jiang, J.; Zhang, X. Attribution of a record-breaking cold event in the historically warmest year of 2023 and assessing future risks. *npj Clim. Atmos. Sci.* **2025**, *8*, 14. https://doi.org/10.1038/s41612-024-00886-w.
28. Zhang, S.; Zeng, G.; Chen, C.; Chen, D. Mechanisms behind consecutive extreme cold spells in Eurasia: Insights from 2023 and historical analysis. *Clim. Dyn.* **2025**, *63*, 179. https://doi.org/10.1007/s00382-025-07639-2.
29. IPCC. *Climate Change 2021—The Physical Science Basis. Contribution of Working Group I to the Sixth Assessment Report of the Intergovernmental Panel on Climate Change*; Masson-Delmotte, V., Zhai, P., Pirani, A., Connors, S.L., Péan, C., Berger, S., Caud, N., Chen, Y., Goldfarb, L., Gomis, M.I., et al., Eds.; Cambridge University Press: Cambridge, UK, 2021. https://doi.org/10.1017/9781009157896.
30. Zhang, X.; Alexander, L.; Hegerl, G.C.; Jones, P.; Klein Tank, A.; Peterson, T.C.; Trewin, B.; Zwiers, F.W. Indices for monitoring changes in extremes based on daily temperature and precipitation data. WIREs *Clim. Change* **2011**, *2*, 851–870. https://doi.org/10.1002/wcc.147.
31. Sillmann, J.; Kharin, V.V.; Zhang, X.; Zwiers, F.W.; Bronaugh, D. Climate extremes indices in the CMIP5 multimodel ensemble: Part 1. Model evaluation in the present climate. *J. Geophys. Res. Atmos.* **2013**, *118*, 1716–1733. https://doi.org/10.1002/jgrd.50203.
32. Gong, Z.Q.; Wang, X.J.; Cui, D.L.; Wang, Y.J.; Ren, F.M.; Feng, G.L.; Zhang, Q.; Zou, X.K.; Wang, X.L. Identification and variation characteristics of regional extreme cold events. *J. Appl. Meteorol. Sci.* **2012**, *23*, 195–204. (In Chinese)
33. Zhu, K.; Lu, W. Elements of climate in China. *Acta Geogr. Sin.* **1935**, *2*, 1–9. (In Chinese)
34. Hersbach, H.; Bell, B.; Berrisford, P.; Hirahara, S.; Horányi, A.; Muñoz-Sabater, J.; Nicolas, J.; Peubey, C.; Radu, R.; Schepers, D.; et al. The ERA5 global reanalysis. *Q. J. R. Meteorol. Soc.* **2020**, *146*, 1999–2049. https://doi.org/10.1002/qj.3803.
35. Feng, T.-C.; Zhang, K.-Q.; Su, H.-J.; Wang, X.-J.; Gong, Z.-Q.; Zhang, W.-Y. Spatiotemporal distribution characteristics and attribution of extreme regional low temperature event. *Chin. Phys. B* **2015**, *24*, 109201. https://doi.org/10.1088/1674-1056/24/10/109201.
36. Zhang, Y.-X.; Liu, Y.-J.; Ding, Y.-H. Identification of winter long-lasting regional extreme low-temperature events in Eurasia and their variation during 1948–2017. *Adv. Clim. Change Res.* **2021**, *12*, 353–362. https://doi.org/10.1016/j.accre.2021.05.005.
37. Choi, H.I. Assessment of Aggregation Frameworks for Composite Indicators in Measuring Flood Vulnerability to Climate Change. *Sci. Rep.* **2019**, *9*, 19371. https://doi.org/10.1038/s41598-019-55994-y.
38. Geen, R.; Thomson, S.I.; Screen, J.A.; Blackport, R.; Lewis, N.T.; Mudhar, R.; Seviour, W.J.M.; Vallis, G.K. An explanation for the metric dependence of the midlatitude jet-waviness change in response to polar warming. *Geophys. Res. Lett.* **2023**, *50*, e2023GL105132. https://doi.org/10.1029/2023GL105132.
39. Hall, R.J.; Hanna, E.; Chen, L. Winter Arctic amplification at the synoptic timescale, 1979–2018, its regional variation and response to tropical and extratropical variability. *Clim. Dyn.* **2021**, *56*, 457–473. https://doi.org/10.1007/s00382-020-05485-y.
40. Francis, J.A.; Vavrus, S.J. Evidence for a wavier jet stream in response to rapid Arctic warming. *Environ. Res. Lett.* **2015**, *10*, 014005. https://doi.org/10.1088/1748-9326/10/1/014005.
41. Panagiotopoulos, F.; Shahgedanova, M.; Hannachi, A.; Stephenson, D.B. Observed trends and teleconnections of the Siberian High: A recently declining center of action. *J. Clim.* **2005**, *18*, 1411–1422. https://doi.org/10.1175/JCLI3352.1.
42. D'Arrigo, R.; Jacoby, G.; Wilson, R.; Panagiotopoulos, F. A reconstructed Siberian High index since A.D. 1599 from Eurasian and North American tree rings. *Geophys. Res. Lett.* **2005**, *32*, L05705. https://doi.org/10.1029/2004GL022271.
43. Wu, B.; Wang, J. Winter Arctic Oscillation, Siberian High and East Asian Winter Monsoon. *Geophys. Res. Lett.* **2002**, *29*, 1897. https://doi.org/10.1029/2002GL015373.
44. Qiao, S.; Zou, M.; Cheung, H.N.; Zhou, W.; Li, Q.; Feng, G.; Dong, W. Predictability of the wintertime 500 hPa geopotential height over Ural-Siberia in the NCEP climate forecast system. *Clim. Dyn.* **2020**, *54*, 1591–1606. https://doi.org/10.1007/s00382-019-05074-8.
45. Takaya, K.; Nakamura, H. Geographical dependence of upper-level blocking formation associated with intraseasonal amplification of the Siberian high. *J. Atmos. Sci.* **2005**, *62*, 4441–4459. https://doi.org/10.1175/JAS3628.1.
46. Li, D.; Zhang, R.; Huang, J. A pitchfork-like relationship between reduced Barents-Kara sea ice and Ural atmospheric circulation. *Clim. Dyn.* **2023**, *61*, 3453–3480. https://doi.org/10.1007/s00382-023-06743-5.
47. Wilks, D.S. *Statistical Methods in the Atmospheric Sciences*, 3rd ed.; Academic Press: Oxford, UK, 2011.
48. Pettitt, A.N. A non-parametric approach to the change-point problem. *Appl. Stat.* **1979**, *28*, 126–135. https://doi.org/10.2307/2346729.
49. Efron, B.; Tibshirani, R.J. *An Introduction to the Bootstrap*; Chapman & Hall: New York, NY, USA, 1993.
50. Cohen, J.; Francis, J.A.; Pfeiffer, K. Anomalous Arctic warming linked with severe winter weather in Northern Hemisphere continents. Commun. *Earth Environ.* **2024**, *5*, 557. https://doi.org/10.1038/s43247-024-01720-0.

51. Zhou, X.; Sato, T.; Li, S. Interannual variation of the Warm Arctic–Cold Eurasia pattern modulated by Ural blocking and the North Atlantic Oscillation under changing sea ice conditions. *Prog. Earth Planet. Sci.* **2023**, *10*, 59. https://doi.org/10.1186/s40645-023-00591-x.
52. Ku, H.-Y.; Wang, M.; Overland, J.; Kim, S.-J.; Yang, G.-H.; Kim, B.-M. Unraveling the Warm Arctic–Cold Eurasia Pattern: Interplay of Arctic Amplification and Internal Variability in Shaping Midlatitude Weather. *J. Clim.* **2025**, *38*, 4975–4987. https://doi.org/10.1175/JCLI-D-24-0599.1.
53. Geng, X.; Noh, K.-M.; Kim, K.; Kug, J.-S. Midwinter breakdown of ENSO climate impacts in East Asia. *npj Clim. Atmos. Sci.* **2023**, *6*, 155. https://doi.org/10.1038/s41612-023-00474-4.

Disclaimer/Publisher's Note: The statements, opinions and data contained in all publications are solely those of the individual author(s) and contributor(s) and not of MDPI and/or the editor(s). MDPI and/or the editor(s) disclaim responsibility for any injury to people or property resulting from any ideas, methods, instructions or products referred to in the content.